A TOG Protein Confers Tension Sensitivity to Kinetochore-Microtubule Attachments

Graphical Abstract
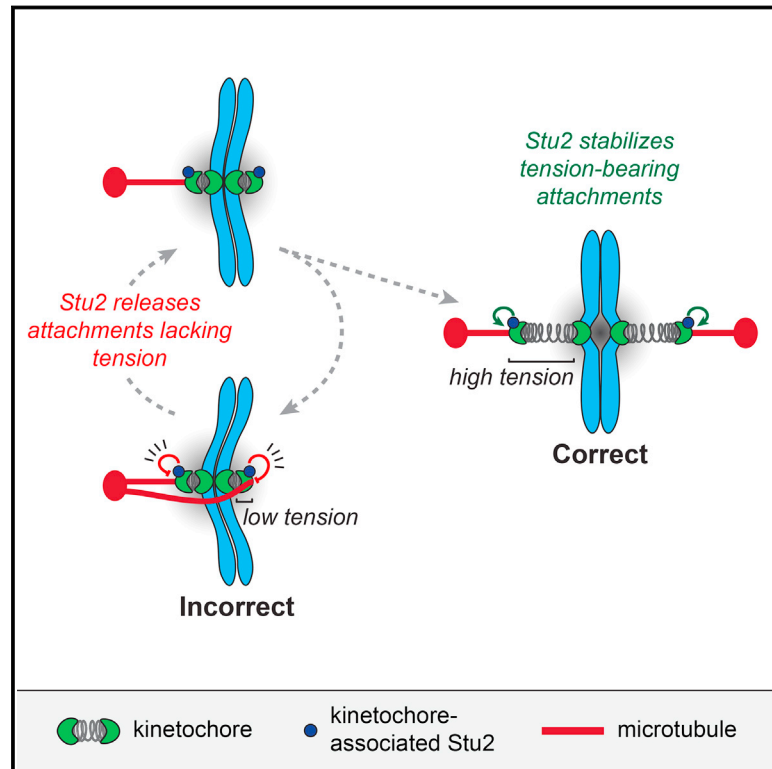
Authors

Matthew P. Miller, Charles L. Asbury, Sue Biggins

Correspondence

casbury@uw.edu (C.L.A.),
sbiggins@fredhutch.org (S.B.)

In Brief

A protein involved in attachment of spindle microtubules to the kinetochore during chromosome segregation selectively stabilizes tension-bearing attachments because its functional output is context dependent: it can either stabilize or destabilize attachments depending on the level of kinetochore tension and the state of the microtubule tip.

Highlights

- ch-TOG and Stu2 exhibit a conserved interaction with the Ndc80 kinetochore complex

- Kinetochore-bound Stu2 directly contributes to microtubule attachment stability

- Stu2's kinetochore function is force and microtubule growth state dependent

- Stu2 selectively stabilizes tension-bearing kinetochore attachments

Article

A TOG Protein Confers Tension Sensitivity to Kinetochore-Microtubule Attachments

Matthew P. Miller,[1] Charles L. Asbury,[2,*] and Sue Biggins[1,*]
[1]Howard Hughes Medical Institute, Division of Basic Sciences, Fred Hutchinson Cancer Research Center, Seattle, WA 98109, USA
[2]Department of Physiology & Biophysics, University of Washington, Seattle, WA 98195, USA
*Correspondence: casbury@uw.edu (C.L.A.), sbiggins@fredhutch.org (S.B.)
 http://dx.doi.org/10.1016/j.cell.2016.04.030

SUMMARY

The development and survival of all organisms depends on equal partitioning of their genomes during cell division. Accurate chromosome segregation requires selective stabilization of kinetochore-microtubule attachments that come under tension due to opposing pulling forces exerted on sister kinetochores by dynamic microtubule tips. Here, we show that the XMAP215 family member, Stu2, makes a major contribution to kinetochore-microtubule coupling. Stu2 and its human ortholog, ch-TOG, exhibit a conserved interaction with the Ndc80 kinetochore complex that strengthens its attachment to microtubule tips. Strikingly, Stu2 can either stabilize or destabilize kinetochore attachments, depending on the level of kinetochore tension and whether the microtubule tip is assembling or disassembling. These dichotomous effects of Stu2 are independent of its previously studied regulation of microtubule dynamics. Altogether, our results demonstrate how a kinetochore-associated factor can confer opposing, tension-dependent effects to selectively stabilize tension-bearing attachments, providing mechanistic insight into the basis for accuracy during chromosome segregation.

INTRODUCTION

Cellular and organismal fitness requires proper partitioning of genetic material during cell division. Failure to accurately segregate chromosomes causes aneuploidy, the most prevalent genetic alteration in tumor cells and a potential factor in the evolution of cancer (reviewed in Gordon et al., 2012). Chromosome segregation is driven by microtubule-based forces, which are generated at kinetochores. The kinetochores must stay bound to microtubule "plus ends," where tubulin subunits are added and lost at a high rate and where the microtubule filaments switch stochastically between phases of assembly and disassembly (Mitchison and Kirschner, 1984).

Kinetochores are conserved macromolecular complexes containing multiple copies of various subcomplexes that assemble onto centromeric DNA (reviewed in Cheeseman, 2014). The major microtubule binding activity within the kinetochore is attributed to the conserved Ndc80 complex (the Ndc80 protein is termed Hec1 in humans) because knockdowns in vivo cause severe defects in kinetochore-microtubule attachment (Cheeseman et al., 2006; DeLuca et al., 2005; McCleland et al., 2004; Wigge and Kilmartin, 2001). However, additional complexes interact with the Ndc80 complex and contribute to attachments, such as the yeast Dam1 complex and its putative functional ortholog, the human Ska complex (Cheeseman et al., 2001; Hanisch et al., 2006; Welburn et al., 2009). While much is understood about how these subcomplexes function alone, it is not known how the activities of these various complexes are coordinated within the larger kinetochore structure. In addition, the extent to which additional kinetochore components contribute to kinetochore-microtubule attachment remains unclear.

To ensure accurate chromosome segregation, sister kinetochores must "biorient," attaching to microtubules from opposite poles, prior to anaphase. Once kinetochores biorient, they come under tension from opposing microtubule pulling forces. Pioneering work showed that incorrect kinetochore attachments are unstable due to the absence of tension (Dietz, 1958; Nicklas and Koch, 1969). The selective release of attachments lacking tension gives the cell another chance to establish proper attachments. While this error correction process relies partly on the Aurora B kinase, which phosphorylates Ndc80 and other kinetochore proteins (reviewed in Carmena et al., 2012; Krenn and Musacchio, 2015), kinetochore-microtubule attachments also possess an intrinsic tension selectivity. Tension directly stabilizes attachments independently of the Aurora B error correction system (Akiyoshi et al., 2010) via two inter-related properties. First, kinetochores bind more stably to assembling tips than to disassembling tips. Second, tension promotes microtubule assembly, which therefore reinforces kinetochore-microtubule attachments at higher forces. Although these properties are sufficient to explain the stabilization of kinetochore-microtubule attachments by tension, specific factors that mediate this activity have not yet been identified.

One conserved family of proteins that localizes to kinetochores and microtubule tips and could therefore contribute to the tension-dependent stabilization of attachments is the XMAP215 family (ch-TOG in humans and Stu2 in budding yeast) (Gard and Kirschner, 1987; He et al., 2001; Hsu and Toda, 2011; Kalantzaki et al., 2015; Ohkura et al., 1988; Tanaka et al., 2005; Tang et al., 2013; Wang and Huffaker, 1997). These proteins generally function as microtubule polymerases by accelerating growth and inhibiting catastrophe (Al-Bassam et al., 2006,

CrossMark

A

Dsn1-His-Flag — + +
Stu2-Myc + − +

Input — Stu2 (α-Myc)

Dsn1 IP
Stu2 (α-Myc)
Dsn1 (α-Flag)
Ctf19 (α-Ctf19)

B

wild-type dad1-1 ndc80-1 spc105-15

Dsn1-His-Flag − + + + + +
Stu2-Myc + − + + + +

Input — Stu2 (α-Myc)

Dsn1 IP
Stu2 (α-Myc)
Dsn1 (α-Flag)

C

Stu2 input | elution

— + + Immobilized Ndc80c
+ − + Stu2 incubation

kDa

200 -
116 -
97.4 -
66 -
45 -
31 -
21.5 -
14.4 -
6.5 -

- Stu2-V5
- Ndc80
I• background
- Nuf2
- Spc24-His-Flag
- Spc25
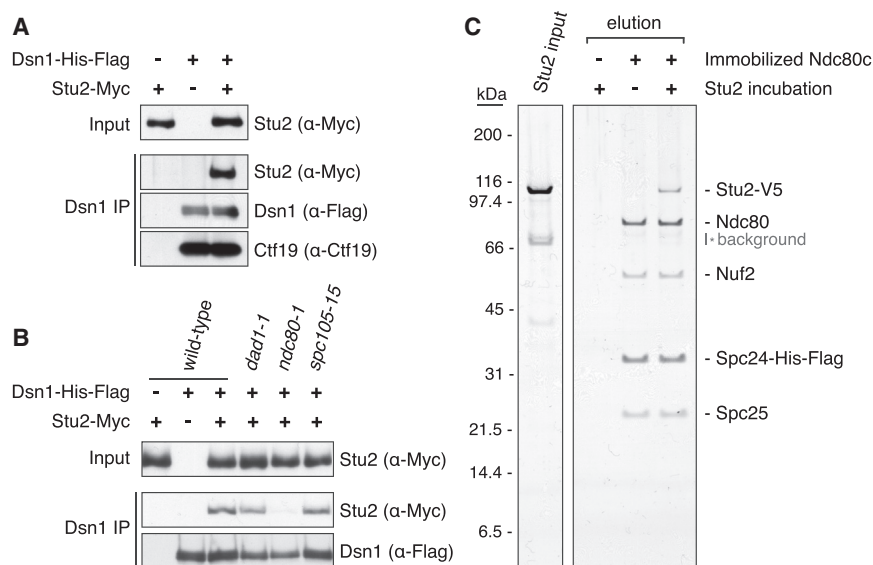
Figure 1. Stu2 Is a Core Kinetochore Component that Associates with the Ndc80 Complex

(A) Protein lysates were prepared from Stu2-13Myc (SBY2861), Dsn1-6His-3Flag (SBY8253), or Stu2-13Myc Dsn1-6His-3Flag (SBY10343) yeast strains. Kinetochore particles were purified by α-Flag immunoprecipitation (IP) and analyzed by immunoblotting. Ctf19 is an inner kinetochore component shown as a control.

(B) Protein lysates prepared from cultures shifted to 37°C (for 2 hr) containing Stu2-13Myc (SBY2861), Dsn1-6His-3Flag (SBY8253), Stu2-13Myc Dsn1-6His-3Flag (SBY10343), or Stu2-13Myc Dsn1-6His-3Flag in combination with the temperature sensitive alleles *dad1-1* (SBY10345), *ndc80-1* (SBY10434), or *spc105-15* (SBY10438). Kinetochore particles were purified by α-Flag IP and analyzed by immunoblotting.

C) Protein lysates prepared from strains containing Stu2-3V5 (SBY11709) and Spc24-6His-3Flag Spc105-AID (SBY14022), respectively. Immobilized Ndc80c-beads were incubated with Stu2-3V5, washed, and eluted with Flag peptide. Control beads lacking Ndc80c were incubated with untagged lysate (from SBY3) prior to incubating with Stu2-3V5. Ndc80c-bound proteins were analyzed by silver stained SDS-PAGE.

2012; Brouhard et al., 2008; Podolski et al., 2014; Widlund et al., 2011), although microtubule-destabilizing activity has also been reported in some contexts (van Breugel et al., 2003; Shirasu-Hiza et al., 2003). They are large proteins that contain highly conserved tumor over-expressed gene (TOG) domain arrays that bind curved tubulin dimers and are thought to accelerate growth by increasing the effective concentration of tubulin subunits near the microtubule plus end (Ayaz et al., 2012, 2014; Fox et al., 2014). They also contain additional functional domains (reviewed in Al-Bassam and Chang, 2011), such as a basic linker that promotes binding to the microtubule lattice. Nearly all XMAP215 orthologs are essential for viability and localize to a variety of microtubule-related structures (reviewed in Al-Bassam and Chang, 2011). Intriguingly, in both yeast and human cells, loss of the XMAP215 family member leads to chromosome alignment defects and to the appearance of detached kinetochores, suggesting a role in attaching kinetochores to microtubules (Gandhi et al., 2011; Gergely et al., 2003; Gillett et al., 2004; Kitamura et al., 2010; Kosco et al., 2001; Marco et al., 2013; Meraldi et al., 2004; Severin et al., 2001). In fission yeast, the XMAP215 homologs bind to the kinetochore and are implicated in regulating microtubule attachments (Hsu and Toda, 2011; Tang et al., 2013). However, these phenotypes are generally assumed to arise indirectly due to their effects on microtubule dynamics. Whether this protein family also participates more directly in kinetochore-microtubule attachment remains uncertain.

Here, we use a reconstitution system to uncover a direct role for the XMAP215 family in kinetochore-microtubule coupling. We show that a conserved interaction between Stu2 and the Ndc80 complex strengthens kinetochore- and Ndc80-based tip attachments in vitro. Surprisingly, this function of kinetochore-associated Stu2 does not require its polymerase activity. Instead, we find that the presence of Stu2 on kinetochores

directly stabilizes their attachments to assembling microtubule tips while destabilizing their attachments to disassembling tips and, furthermore, that these activities are force dependent. These activities of Stu2 that depend on force and the state of the microtubule tip impart tension selectivity to the kinetochore, enabling it to remain attached to the microtubule for longer durations when tension is increased. Together, our findings suggest that kinetochore-associated Stu2 activity is critical for tuning kinetochore function to make proper microtubule attachments, providing mechanistic insight into the manner in which tension promotes accurate chromosome segregation.

RESULTS

Stu2 Kinetochore Association Depends on an Interaction with the Ndc80 Complex

We previously detected Stu2 co-purifying with native yeast kinetochores by mass spectrometry (Akiyoshi et al., 2010), suggesting it might contribute to the activity of reconstituted kinetochore-microtubule interactions in vitro. To begin analyzing this, we first confirmed that Stu2 is present on isolated kinetochore particles. Native kinetochores are isolated from budding yeast cells via single-step immunoprecipitation of the Mis12/MIND/Mtw1 complex component Dsn1-His-Flag (Akiyoshi et al., 2010). These kinetochore particles contain the "core" kinetochore components but lack tubulin and some other transiently associated factors (Akiyoshi et al., 2010). We confirmed that Stu2 is present on isolated kinetochores by immunoblotting (Figure 1A).

To understand how Stu2 localizes to kinetochores in the absence of microtubules, we identified the subcomplex required for Stu2-kinetochore association. Kinetochore particles were purified from cells carrying temperature-sensitive alleles

A

WT

stu2-AID

stu2-AID + STU2

YPD + DMSO

YPD + auxin

C

- bi-lobed
- mono-lobed
- unattached

B

DIC   DAPI   Mtw1   Tub1   merge

cdc20-AID — bi-lobed

cdc20-AID stu2-AID — bi-lobed, mono-lobed, unattached

D

DIC   DAPI   GFP   merge

correct

mis-segregated

E

- correct
- mis-segregated
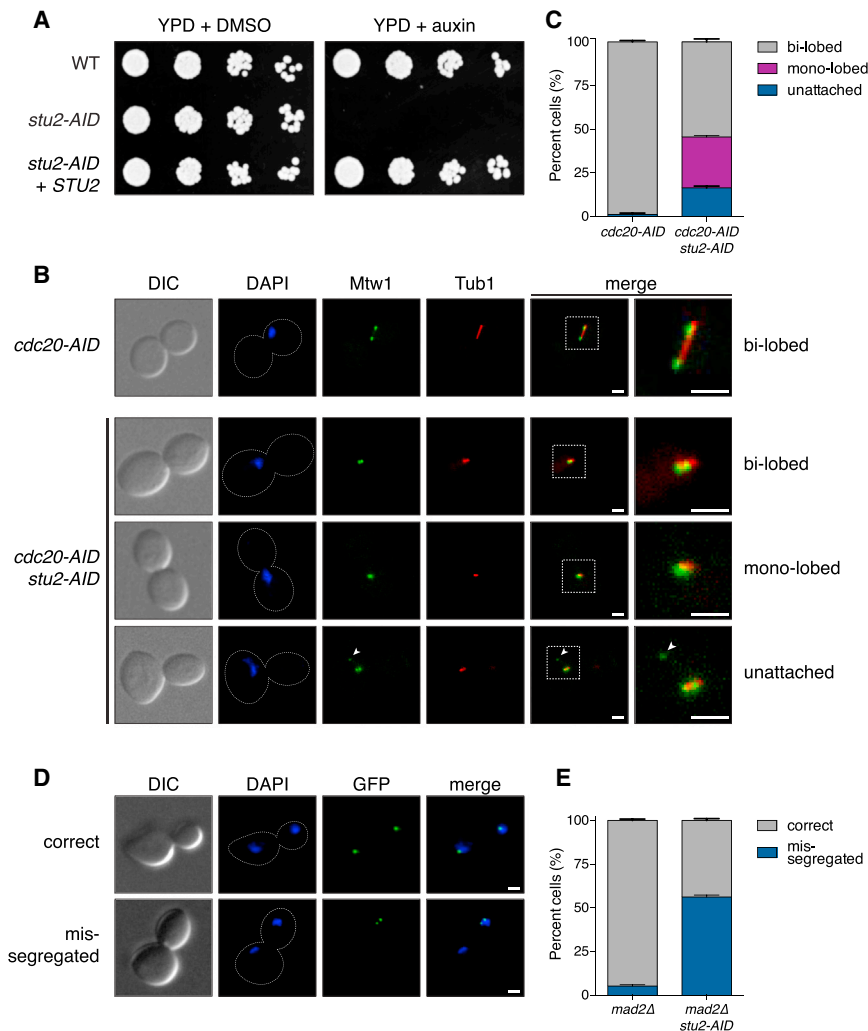
Figure 2. Cells Lacking Stu2 Have Kineto-chore-Microtubule Attachment Defects

(A) Wild-type (SBY3), *stu2-AID* (SBY13772), and *stu2-AID* cells expressing *STU2-3V5* from an ectopic locus (SBY13901) were serially diluted (5-fold) and spotted on yeast extract peptone plates containing either DMSO or auxin.

(B) Exponentially growing *cdc20-AID MTW1-3GFP TUB1-CFP* (SBY15985) cultures, or also containing *stu2-AID* (SBY15986), were treated with auxin for 2.5 hr, then fixed and analyzed for Mtw1-3GFP (kinetochore) localization and spindle morphology (Tub1-CFP). Representative images of *cdc20-AID* (wild-type) and *cdc20-AID stu2-AID* cells arrested in metaphase (*cdc20-AID* was used as a control to ensure all strains arrested in metaphase). Mtw1 (green) localization was categorized as bi-lobed, mono-lobed, or unattached (off the spindle axis; white arrow head). DAPI-stained DNA is shown in blue, and Tub1-CFP is shown in red. Boxed regions are magnified and shown in the rightmost columns. White bars for (B) and (D) represent 2 μm.

(C) Quantification of Mtw1 localization from (B). Error bars represent SD of three independent experiments; n = 200 cells for each experiment.

(D) Exponentially growing *mad2Δ* (SBY468) or *mad2Δ stu2-AID* (SBY16236) cells containing fluorescently labeled chromosome IV were released from a G1 arrest into auxin containing media. Representative images of *mad2Δ* (correct segregation) and *mad2Δ stu2-AID* (missegregated) cells are shown. DAPI-stained DNA is shown in blue, and LacI-GFP (marking chromosome IV) is shown in green.

(E) Quantification of chromosome segregation in anaphase from (D). Error bars represent SD of three independent experiments; n = 200 cells for each experiment.

of a component of the Dam1 (*dad1-1*), Ndc80 (*ndc80-1*), or KNL1[Spc105] (*spc105-15*) complexes. The Stu2 kinetochore-association was disrupted only in cells carrying an *ndc80-1* allele (Figure 1B), in agreement with previously reported chromatin immunoprecipitation data (He et al., 2001; Ma et al., 2007). We further confirmed this by isolating kinetochores from cells carrying an *ndc80-AID* (auxin inducible degron; Nishimura et al., 2009) allele, indicating there is a kinetochore-bound pool of Stu2 that requires the Ndc80 complex for its association (Figure S1A).

Stu2 Binds Directly to the Ndc80 Complex In Vitro

Although the fission yeast Stu2 homologs interact with the Ndc80 complex (Hsu and Toda, 2011; Tang et al., 2013), the budding yeast Stu2 and Ndc80 proteins were reported to not interact in a yeast two-hybrid assay (Maure et al., 2011). We therefore directly tested whether Stu2 and Ndc80 complex (Ndc80c) associate. We independently isolated them via single-step immunoprecipitation of Stu2-V5 or an Ndc80c component, Spc24-His-Flag, followed by high-salt washes to remove

co-purifying proteins (Figures 1C and S1B). These conditions result in the isolation of the heterotetrameric Ndc80c or Stu2 to high purity (Figures 1C). We then incubated immobilized Ndc80c with purified Stu2-V5 and detected a specific interaction (Figures 1C and S1D), suggesting that Stu2 associates with kinetochores via Ndc80c.

Kinetochore-Associated Stu2 Makes a Major Contribution to Attachment Strength

To analyze the function of Stu2 at kinetochores, we generated cells containing a *stu2-AID* allele at the endogenous locus that targets the protein for degradation when the TIR1 F-box protein and the hormone auxin are present (Nishimura et al., 2009). Under these conditions, the Stu2-AID protein is rapidly degraded (Figure S2A) and the cells are inviable (Figure 2A). To determine whether these Stu2-depleted cells display a defect in kinetochore-microtubule attachments in vivo, as previously observed in various *stu2* mutants (Gandhi et al., 2011; Gillett et al., 2004; Kitamura et al., 2010; Kosco et al., 2001; Marco et al., 2013; Severin et al., 2001), we examined spindle

morphology and kinetochore distribution by fluorescence microscopy. In budding yeast, properly attached bioriented kinetochores cluster and exhibit a characteristic bi-lobed distribution at metaphase when they come under tension (Goshima and Yanagida, 2000; He et al., 2000; Pearson et al., 2001). As expected, when cells were arrested in metaphase (using a *cdc20-AID* strain) nearly all had a bipolar spindle and bi-lobed kinetochore foci (Figures 2B and 2C; 98% ± 1%). In contrast, cells depleted of Stu2 (*cdc20-AID stu2-AID*) arrested with an abnormally short bipolar spindle and three classes of kinetochore configurations (Figure 2B; Kosco et al., 2001; Marco et al., 2013; Pearson et al., 2003; Severin et al., 2001). 55% ± 2% of the cells had normal bi-lobed kinetochore foci, albeit less discrete due to the dramatically shorter spindle. However, 29% ± 1% arrested with a single kinetochore focus and 16% ± 1% showed clear kinetochore-microtubule attachment defects judged by a kinetochore signal off the spindle axis (Figures 2B and 2C).

To monitor chromosome segregation after Stu2 depletion, we fluorescently marked chromosome IV (Straight et al., 1996) and also deleted a component of the spindle checkpoint to allow *stu2* mutants to progress into anaphase (Figure S2B; Severin et al., 2001). Nearly all cells containing Stu2 function (*mad2Δ*) properly segregated a copy of chromosome IV to each daughter nucleus (Figures 2D and 2E; 95% ± 1%). However, cells depleted of Stu2 (*stu2-AID mad2Δ*) displayed high rates of chromosome missegregation, with 56% ± 1% of anaphase cells containing GFP signal in only one of two nuclei (Figures 2D and 2E). Together, these data confirm that cells lacking Stu2 have defective kinetochore-microtubule interactions.

To determine whether the population of Stu2 specifically associated with the kinetochore mediates microtubule attachment, we analyzed the attachment strength of kinetochore particles in vitro. Kinetochores purified from Stu2-depleted cells (Stu2-AID) lacked Stu2, but otherwise appeared intact as judged by overall protein composition (Figures 3A and 3B). To measure kinetochore strength, we used an optical trapping-based "force-ramp" technique, where kinetochores were linked to beads and then attached to growing microtubule ends using the laser trap (Figure 3C; reviewed in Franck et al., 2010). The instrument was then programmed to increase force across the kinetochore-microtubule interface until the attachment ruptured (Figure 3D). For consistency, rupture force measurements were always made from assembling microtubule tips at kinetochore concentrations we previously showed monitored single kinetochore-microtubule attachments (Akiyoshi et al., 2010). Individual wild-type kinetochores ruptured at an average of 9.1 ± 0.5 pN, equivalent to the previous measurements of wild-type particles (Akiyoshi et al., 2010). In contrast, Stu2-depleted kinetochores were significantly weaker, rupturing at an average of 4.3 ± 0.3 pN (Figure 3E). This decrease is similar to that observed for kinetochores lacking the Dam1 complex, which rupture at 2.8 ± 0.2 pN on average (Figure S3; Akiyoshi et al., 2010). Thus, the absence of Stu2 weakens kinetochore attachments nearly as much as the loss of the Dam1 complex, which is widely considered to be a crucial microtubule attachment factor (reviewed in Nogales and Ramey, 2009).

To determine whether the reduced strength is due solely to the loss of Stu2, we tested whether the addition of purified Stu2 could reconstitute microtubule attachment strength. First, we confirmed that purified Stu2 binds kinetochore particles in an Ndc80c-dependent manner (Figures S4A and S4B). Next, we measured rupture force distributions for wild-type and Stu2-depleted kinetochore particles preincubated with purified Stu2-Flag (Figure S1C). The addition of Stu2 completely reconstituted the attachment strength of Stu2-depleted kinetochore particles (9.2 ± 0.7 pN) while not affecting the rupture force of wild-type particles containing endogenous Stu2 (9.6 ± 0.6 pN; Figure 3E). Together, these results show that kinetochore-bound Stu2 significantly contributes to the overall attachment strength of purified kinetochore particles.

Stu2 Directly Strengthens Ndc80-Based Attachments

If Stu2 strengthens kinetochores via its association with Ndc80c, we reasoned that it might also strengthen tip attachments formed by Ndc80c alone. When Ndc80c (described in Figure 1C) was bound to polystyrene beads at sufficiently high density, such that multiple complexes could engage simultaneously with the microtubule tip, it maintained attachments to growing microtubule tips with an average rupture strength of 3.7 ± 0.3 pN as previously seen (Figure 3F; Powers et al., 2009). The addition of purified Stu2 increased the rupture strength of these Ndc80c-coated beads dramatically, to an average of 10.6 ± 0.6 pN (Figure 3F). We observed similar results using recombinant Ndc80c instead of native Ndc80c purified from yeast (data not shown). The *Xenopus* Stu2 family member XMAP215 alone forms load-bearing attachments to dynamic microtubule tips (Trushko et al., 2013), suggesting that Stu2 by itself might also possess an inherent tip-coupling activity. To test this, we measured rupture force distributions for Stu2-decorated beads and found an average strength of 3.8 ± 0.6 pN (Figures S4C and S4D). Together, these results demonstrate that Stu2 binding to Ndc80c enhances tip coupling, possibly through the addition of its own inherent microtubule binding activity.

Conserved Enhancement of Ndc80c Activity via an Interaction with ch-TOG

To examine whether the orthologous human proteins also interact, we incubated recombinant Hec1/Ndc80c with immobilized recombinant ch-TOG and found a specific association (Figures 4A and S5). To test whether ch-TOG affects the strength of Hec1/Ndc80c-based attachments, we linked purified Hec1/Ndc80 complex to polystyrene beads and measured rupture force distributions in the presence or absence of ch-TOG. Human Hec1/Ndc80c forms a significantly stronger microtubule attachment relative to the yeast Ndc80c under these conditions (average rupture strength of 12.7 ± 1.3 pN for human versus ∼4 pN for yeast), for reasons that are unknown. Nevertheless, the addition of purified ch-TOG led to a statistically significant increase in rupture strength, to an average of 16.3 ± 1.0 pN (Figure 4B). Thus, the association with kinetochores and the strengthening of kinetochore-tip attachments appear to be conserved activities shared by the yeast and human orthologs, Stu2 and ch-TOG.
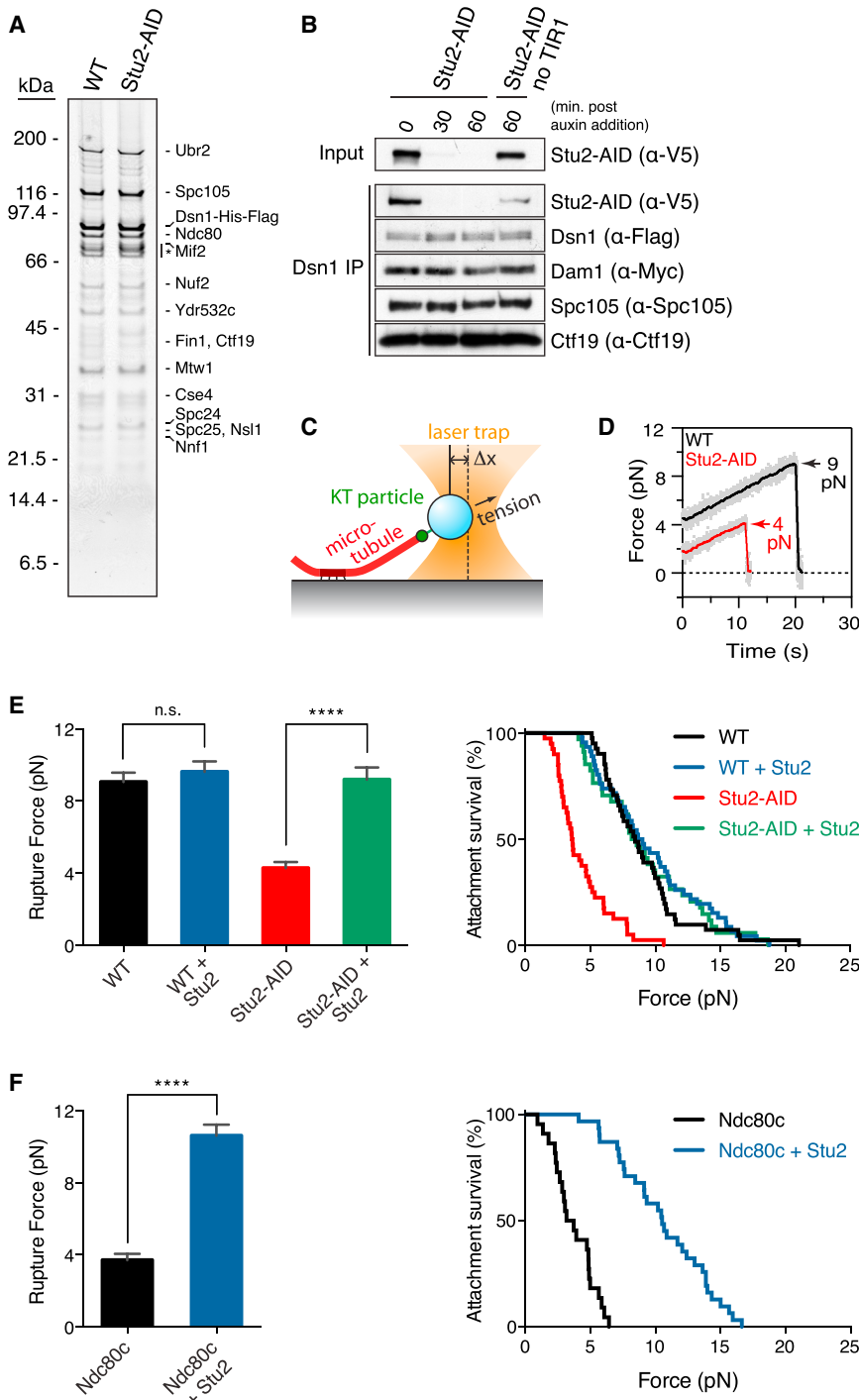
Figure 3. Kinetochore-Associated Stu2 Significantly Contributes to the Attachment Strength of Purified Kinetochore Particles

(A) Protein lysates prepared from Dsn1-6His-3Flag (SBY8253) or Dsn1-6His-3Flag Stu2-AID (SBY13772) strains. SBY13772 was treated with auxin for 30 min prior to harvesting cells. Kinetochore particles were purified by α-Flag immunoprecipitation and analyzed by SDS-PAGE and silver stain analysis. Note that co-purified Stu2 is not visible by silver stain analysis at this concentration.

(B) Exponentially growing Stu2-AID (SBY11856) or Stu2-AID lacking TIR1 (SBY11858) cultures that also contained Dsn1-6His-3Flag and Dam1-9Myc were treated with auxin. Protein lysates were prepared 0, 30, or 60 min post auxin addition and kinetochore particles were purified by α-Flag immunoprecipitation (IP) and analyzed by immunoblotting.

(C) Schematic of optical trap assay. Dynamic microtubules are grown from coverslip-anchored seeds. Purified kinetochores are linked to beads via Dsn1 and are manipulated using an optical trap to exert applied force across the kinetochore-microtubule interface.

(D) Representative records of applied force versus time for wild-type (black) or Stu2-AID (red) kinetochore particles bound to assembling microtubule tips. Applied force was increased at a rate of 0.25 pN s^{-1} until attachment rupture (marked by arrows). Gray points show raw data. Colored traces show the same data after smoothing with a 500 ms sliding boxcar average.

(E) Left: mean rupture forces for wild-type or Stu2-AID kinetochore particles either untreated or pre-incubated with Stu2-Flag. Error bars in (E) and (F) represent SEM (n = 22–46 events). p values in (E) and (F) were determined using a two-tailed unpaired t test (n.s., not significant; ****p < 0.0001). Right: attachment survival probability versus force for the same data.

(F) Left: mean rupture forces for Ndc80c-linked beads untreated or incubated with Stu2-3V5. Right: attachment survival probability versus force for the same data.

based "force-clamp" assay. As before, bead-bound kinetochores were attached to microtubule tips using an optical trap. However, rather than gradually increasing the force, we instead applied fixed levels of tension in the direction of microtubule growth. In this assay, kinetochores track continuously with tip growth and shortening, allowing us to monitor the dynamic instability of kinetochore-attached microtubules with high spatiotemporal resolution (Figures 5A and 5B; Akiyoshi et al., 2010). We examined a range of forces (from 1 to 5 pN) and compared growth and shortening speeds as well as switch rates (catastrophe and rescue frequencies) for microtubule tips attached to kinetochores that either contained or lacked Stu2 (wild-type or Stu2-AID kinetochores, respectively).

Stu2 Did Not Contribute to Tension-Induced Changes in Microtubule Dynamics

Because Stu2 is a microtubule polymerase (Podolski et al., 2014), its role at the kinetochore might be mediated through changes in the dynamics of kinetochore-attached microtubules, as previously proposed (Hsu and Toda, 2011; Tang et al., 2013). To address this, we used an optical trapping-

A

B
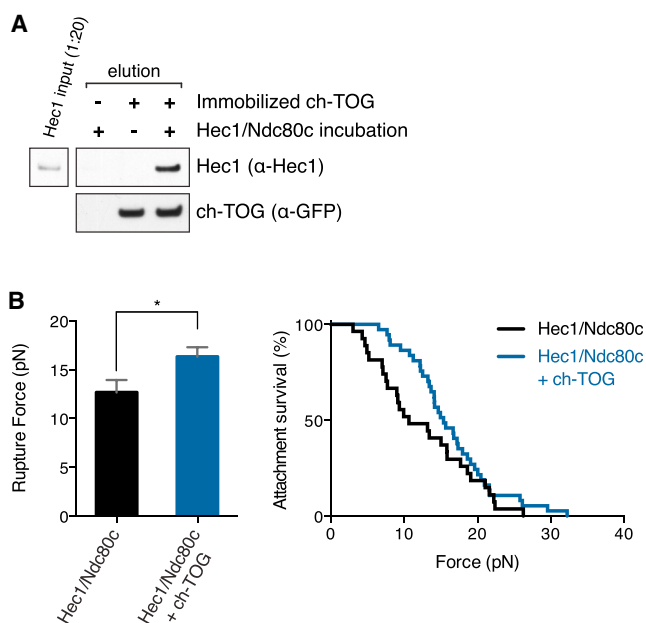
Figure 4. ch-TOG Contributes to the Attachment Strength of Purified Hec1/Ndc80c

(A) GFP-tagged ch-TOG was immobilized by α-GFP IP. Immobilized ch-TOG-beads were incubated with Hec1/Ndc80c, washed, and eluted in sample buffer. ch-TOG-bound proteins were analyzed by immunoblotting.

(B) Left: Mean rupture forces for Hec1/Ndc80 complex-linked beads untreated or incubated with ch-TOG. Error bars represent SEM (n = 27–37 events). p value was determined using a two-tailed unpaired t test (p = 0.024). Right: attachment survival probability versus force for the same data.

For microtubules attached to wild-type kinetochores, the growth speeds and rescue rates increased with tension, while the shortening speeds and catastrophe rates decreased with tension, consistent with our previous observations using recombinant components or native kinetochores (Akiyoshi et al., 2010; Franck et al., 2007). Surprisingly, however, when attached to kinetochores lacking Stu2, the microtubules behaved indistinguishably from those attached to kinetochores that retained Stu2. We found no clear differences in any of the four dynamic rate parameters for microtubules attached to Stu2-AID kinetochores versus wild-type kinetochores (Figures 5C and 5D), measured over the full range of experimentally accessible forces. Thus, the kinetochore-bound pool of Stu2 does not contribute to the tension-induced changes in microtubule dynamics that we observe in vitro.

Stu2 Has Dichotomous Effects on Attachment Stability

Although kinetochore-attached microtubule dynamics were unaffected by the absence of Stu2, the stability of kinetochore-microtubule coupling clearly was affected. Kinetochore particles lacking Stu2 detached more frequently from assembling tips than wild-type particles at all forces examined (Figure 5E), consistent with our rupture force experiments (Figures 3E and 3F). Furthermore, this difference was magnified at higher forces, indicating that, during tip growth, the contribution of Stu2 to attachment stability was enhanced by tension. During tip short-

ening, the effect of Stu2 was also force dependent but, remarkably, its contribution was reversed—when examined at low tension (≤ 2 pN), kinetochores lacking Stu2 detached *less* frequently from disassembling tips than wild-type particles, indicating that the presence of Stu2 can *destabilize* attachments specifically during tip shortening (Figure 5F). This Stu2-dependent destabilization during tip shortening was suppressed by tension. Together, these results show that Stu2 affects kinetochore-microtubule attachment stability in a manner that depends on the state of the microtubule tip and on the level of kinetochore tension.

Stu2 Underlies Selective Stabilization of Tension-Bearing Kinetochore Attachments

We previously showed that the overall lifetime of reconstituted kinetochore-microtubule attachments varies biphasically with tension, initially increasing with force, reaching an optimum at ~5 pN, and then decreasing as the force is raised further (Akiyoshi et al., 2010). This intrinsic selectivity for tension-bearing attachments occurs because tension inhibits microtubule disassembly (mainly by suppressing catastrophes) and because the kinetochores detach far less frequently from assembling than from disassembling tips. Our discovery that Stu2 alters the tension dependence of detachment frequencies (Figures 5E and 5F) suggested that it might also contribute to the intrinsic tension selectivity of kinetochores. We therefore examined how the presence or absence of kinetochore-associated Stu2 affects the overall attachment lifetime-versus-force relationship. Consistent with our previous observations (Akiyoshi et al., 2010), increasing tension from 1 to 5 pN increased mean attachment lifetimes for wild-type kinetochores 3-fold, from 20 ± 4 to 58 ± 16 min (Figures 6A, 6B, and S6). Strikingly, this tension-dependent stabilization was completely abolished for kinetochores lacking Stu2. Their mean attachment lifetimes decreased monotonically with increasing force, from 34 ± 11 min at 0.9 pN down to 8.5 ± 1.3 min at 2.8 pN (Figure 6B), indicating that Stu2 is essential for the tension selectivity of reconstituted kinetochore-microtubule attachments.

To understand why Stu2 depletion abolishes tension selectivity, we analyzed the force-clamp data using a simple two-state kinetic model (Akiyoshi et al., 2010). The model predicts mean attachment lifetimes given catastrophe and rescue frequencies for a kinetochore-attached microtubule (i.e., rates k_1 and k_2, respectively; Figures 5B and 5D) and given kinetochore detachment frequencies during tip growth and shortening (k_3 and k_4; Figures 5E and 5F). We fit the force-dependence of all four rates with exponential curves and found that the detachment rates (k_3 and k_4) for Stu2-depleted kinetochores were more force sensitive (i.e., fit by steeper curves, with more positive slopes in Figures 5E and 5F), and the unloaded detachment rate during disassembly was also significantly reduced (i.e., lower y-intercept in Figure 5F) relative to wild-type. We found that by changing only the detachment rates (k_3 and k_4) of our model, the predicted lifetime-versus-force curve decayed monotonically with force, providing an excellent fit to the measured lifetimes (see red curve, Figure 6B). Thus, the Stu2-dependent changes in detachment rates alone are sufficient

A

B

C

D

E

F
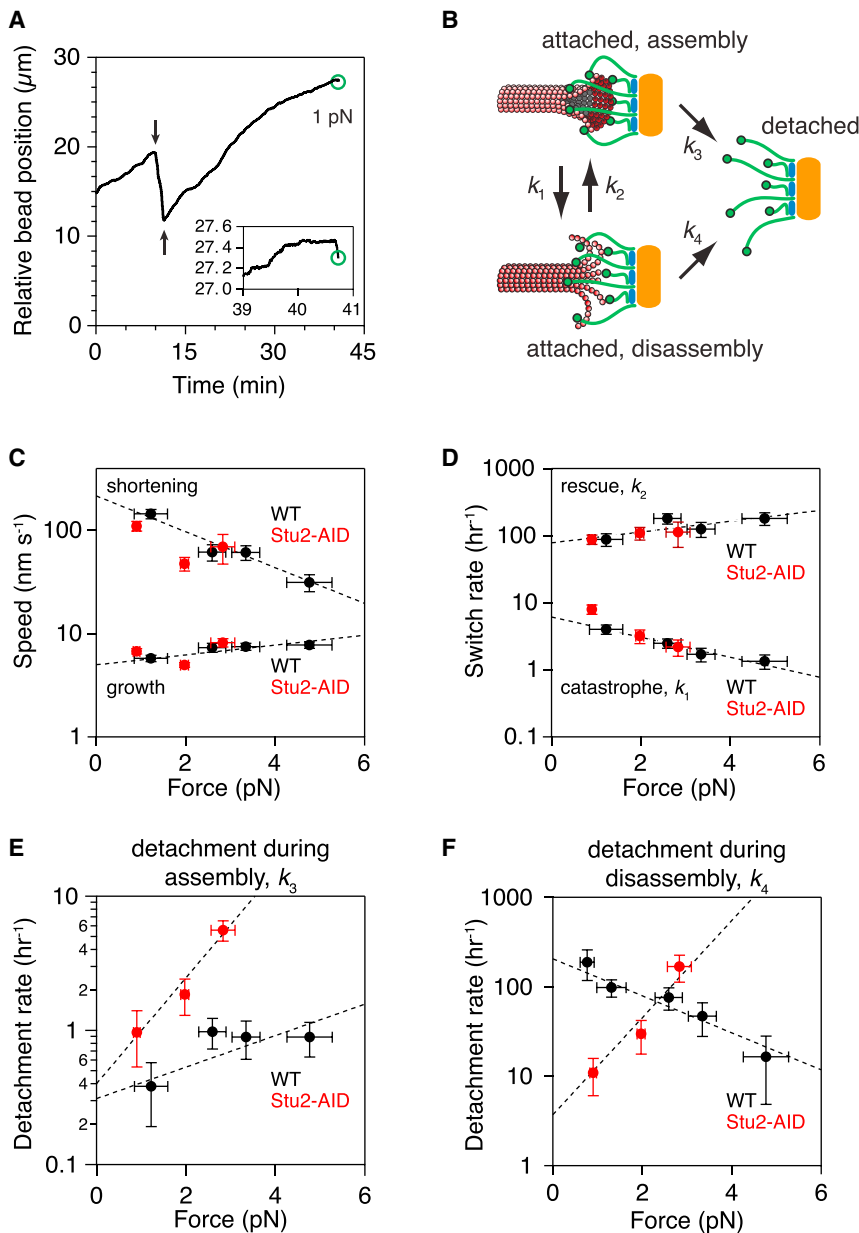
Figure 5. Kinetochore-Associated Stu2 Affects Attachment Stability without Altering Microtubule Dynamics

(A) Representative record of position versus time for wild-type (SBY8253) kinetochore particles subjected continuously to 1.0 ± 0.1 pN of force. Increasing position represents movement coupled to microtubule tip assembly. Decreasing position represents movement driven by tip disassembly. Arrows indicate catastrophes (↓) and rescues (↑). Green circles indicate detachment of the bead from the microtubule tip. Inset shows detachment event at higher resolution, illustrating that it occurred during tip disassembly.

(B) Schematic of two-state model with detachment during assembly and disassembly (rates k_3 and k_4, respectively), and the interconversion between the assembly and disassembly states (k_1 and k_2).

(C–F) Measured rates of microtubule assembly and disassembly (growth and shortening, C), microtubule catastrophe and rescue (k_1 and k_2, D), kinetochore detachment during microtubule assembly (k_3, E), and kinetochore detachment during microtubule disassembly (k_4, F), for wild-type (black) and Stu2-AID (red) kinetochore particles subjected continuously to indicated amount of force. For (C) and (D), exponential fits shown are for wild-type kinetochore particles. For (E) and (F), exponential fits for both wild-type and Stu2-AID are shown. Error bars represent uncertainty due to counting statistics (n = 5–92 events). Wild-type data were combined with wild-type data from Akiyoshi et al. (2010) (see Figure S6).

associated Stu2 as a state-sensitive attachment factor that underlies kinetochore mechano-sensitivity to ensure accurate chromosome segregation.

XMAP215 Homologs Contribute Directly to Kinetochore-Microtubule Coupling

The major function ascribed to XMAP215 family members is promoting microtubule assembly via polymerase activity (reviewed in Al-Bassam and Chang, 2011). Although cells lacking Stu2 or ch-TOG

to explain the tension selectivity observed with wild-type kinetochores.

DISCUSSION

The faithful execution of chromosome segregation is an essential event during cell division and requires the tension-dependent stabilization of properly bioriented kinetochore-microtubule attachments prior to anaphase. Here, we report a previously unknown function for the conserved Stu2 protein in directly regulating kinetochore-microtubule attachments. Remarkably, the kinetochore-associated function of Stu2 is force dependent and serves to selectively stabilize tension-bearing attachments. Together, our data identify kinetochore-

display chromosome alignment defects and unattached kinetochores (Gandhi et al., 2011; Gergely et al., 2003; Gillett et al., 2004; Kosco et al., 2001; Marco et al., 2013; Meraldi et al., 2004; Severin et al., 2001), it has not been clear whether these phenotypes are consequences of general defects in microtubule dynamics or whether they might reflect a more specific function at the kinetochore. Here, by reconstituting kinetochore-microtubule interactions in vitro, we specifically investigated the role of kinetochore-associated Stu2. We find that Stu2 makes a large, direct contribution to the strength of kinetochore-microtubule coupling and, furthermore, that this previously uncharacterized function of Stu2 is likely conserved and separable from its role in regulating microtubule dynamics. These data suggest that a fraction of the cellular pool of Stu2 behaves as a "core"
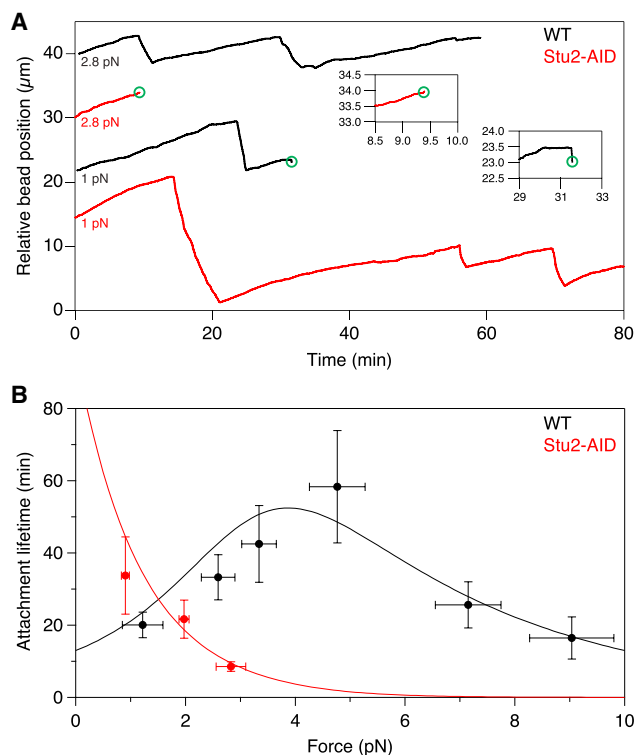
Figure 6. Stu2 Mediates Tension-Dependent Stabilization of Kinetochore-Microtubule Interactions

(A) Representative records of position versus time for wild-type (black, SBY8253) and Stu2-AID (red, SBY11860) kinetochore particles subjected continuously to 1.0 ± 0.1 pN or 2.8 ± 0.1 pN of force (as described in Figure 5A). Insets show detachment events at higher resolution. Attachment duration increases with force for wild-type but decreases with force for Stu2-AID kinetochores. For clarity, traces are offset vertically.

(B) Measured attachment lifetimes for wild-type (black) and Stu2-AID (red) kinetochore particles subjected continuously to indicated amount of force. Curves show prediction of the two-state model (see text). Error bars represent uncertainty due to counting statistics (n = 5–92 events).

kinetochore component that associates stably with the Ndc80 complex to strengthen kinetochore attachments to dynamic microtubule tips, consistent with previous work that detected Stu2 in close proximity and at near-stoichiometric levels with the Ndc80 complex (Aravamudhan et al., 2014).

There are a number of possible mechanisms that could explain how Stu2 strengthens kinetochore-microtubule attachments. Purified Stu2 alone can couple beads to dynamic microtubule tips in vitro, similar to the family member XMAP215 (Trushko et al., 2013), suggesting that these proteins might bring additional direct microtubule binding activity to the kinetochore. Alternatively, Stu2 might alter Ndc80c function, either by allosterically promoting the interaction of Ndc80c with the microtubule or by influencing microtubule tip structure in a way that enhances Ndc80c attachment. Regardless of the underlying mechanism, our work shows that the contribution of Stu2 to kinetochore attachment strength is significant, and similar to that of the Dam1 complex, which is widely considered to be a major kinetochore-microtubule coupling factor (reviewed in Nogales and

Ramey, 2009). These results could explain why mutations in Ndc80c cause severe kinetochore-microtubule attachment defects in vivo even though the in vitro microtubule-binding activity of purified Ndc80c alone is relatively weak. Because Ndc80c recruits both Stu2 and Dam1c to the kinetochore, its phenotypes in vivo reflect the mislocalization of multiple microtubule couplers.

The microtubule polymerization rates in our assays were unaffected by kinetochore-associated Stu2, even though it was in the vicinity of the microtubule tips. It is possible that the effective concentration of Stu2 at kinetochores might be below what is required to promote microtubule assembly or that the orientation of kinetochore-associated Stu2 is incompatible with its polymerase function. Alternatively, the use of mammalian tubulin, which is a poorer substrate for Stu2's microtubule polymerase function (Podolski et al., 2014), might have masked this activity. An important, technically challenging goal for the future will be to measure how kinetochore-associated Stu2 affects the dynamics of microtubules grown from conspecific yeast tubulin. Nevertheless, we have observed dramatic changes in the stability of kinetochore-microtubule attachments under conditions where no detectable changes in microtubule dynamics occurred. Therefore, our work shows that Stu2 plays a critical and hitherto underappreciated role in regulating kinetochore-microtubule attachments.

The Effects of Kinetochore-Associated Stu2 on Attachment Stability Are Regulated by Tension

Stu2 confers opposite effects on kinetochore-microtubule attachment stability depending on the level of tension and on the state of the microtubule tip. It is not yet possible to assign these Stu2-dependent effects to established structural features of the kinetochore-microtubule interface, because kinetochore-microtubule coupling remains poorly understood in mechanistic detail. However, some candidate mechanisms are suggested by the selective binding of Stu2 and Ndc80c to curved and straight conformations of tubulin, respectively (Alushin et al., 2010; Ayaz et al., 2012, 2014), and by the presumed arrangements of these tubulin conformations at the assembling and disassembling tips of kinetochore-attached microtubules. We speculate that by selectively binding curved tubulins at the tip, kinetochore-associated Stu2 might form microtubule links that do not interfere with Ndc80c, which binds straight tubulins that are presumably located within the microtubule lattice (Figure 7A). Faster tip growth at higher tension could increase the number of curved tubulins at the tip, thereby enhancing the contribution of Stu2 to kinetochore attachment stability. During tip disassembly at low tension, the kinetochore-associated Stu2 has a destabilizing effect on attachment. Under these conditions it may directly compete with or occlude the microtubule-binding activities of other kinetochore components (such as Ndc80c; Figure 7B), or it may alter the structure of the disassembling tip in a manner that inhibits their binding. In any case, the interference by Stu2 is relieved as tension is increased. A speculative explanation is that tension-dependent stretching of the kinetochore structure itself might relieve this inhibition by spatially separating Stu2 from the other microtubule-binding kinetochore elements (Figure 7B). Regardless of the mechanism, our observation that Stu2 affects attachment stability in a direct and tension-dependent manner
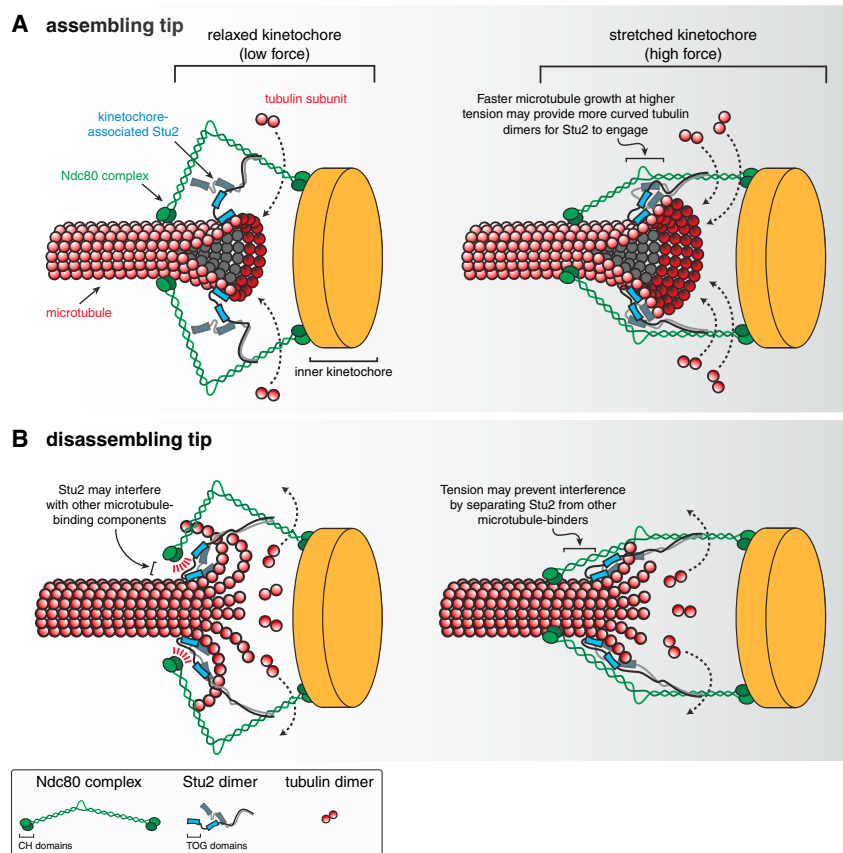
Figure 7. Model of Stu2's Role in Selectively Stabilizing Tension-Bearing Kinetochore-Microtubule Attachments

Stu2's kinetochore function is directly modulated both by tension and the assembly state of the microtubule tip. These activities impart mechano-sensitivity to the kinetochore, which results in the direct stabilization of tension-bearing attachments.

(A) Left: kinetochore-associated Stu2 might specifically bind to curved tubulin subunits at the assembling tip to form additional microtubule links that do not interfere with the Ndc80c (which binds straight tubulins within the microtubule lattice). Alternately, Stu2 could allosterically enhance the ability of the Ndc80c to bind to the microtubule tip or strengthen the attachment indirectly by altering the microtubule tip structure to promote kinetochore binding. Right: the faster growth at high levels of tension might bring more curved tubulin dimers to the growing tip, thereby allowing more Stu2 molecules to engage. A hypothetical arrangement of kinetochore-bound Stu2 is shown based on data from Aravamudhan et al. (2014). For simplicity, only Ndc80c and Stu2 are depicted.
(B) Left: at low levels of tension, Stu2 impedes kinetochore attachment to disassembling microtubule tips, perhaps by occluding the Ndc80c from microtubule binding. Right: at high levels of tension, the increased force across the kinetochore-microtubule interface may alter the kinetochore and/or straighten protofilaments at the microtubule tip. Under these conditions, the destabilizing activity of Stu2 is suppressed.

implicates it as a mechanically regulated element of the kinetochore-microtubule interface.

Stu2 Function Underlies the Intrinsic Selectivity of Kinetochores for Tension-Bearing Attachments

Although tension-dependent stabilization is widely accepted as the basis for mitotic accuracy, how tension stabilizes kinetochore-microtubule attachments remains unclear. The Aurora B kinase promotes the release of erroneous attachments through phosphorylation of various kinetochore components (reviewed in Carmena et al., 2012; Krenn and Musacchio, 2015). However, we previously discovered that kinetochores exhibit an intrinsic selectivity for tension-bearing attachments that is independent of Aurora B (Akiyoshi et al., 2010). Our current results now show that kinetochore-associated Stu2 is a key component of this direct mechano-sensitivity. By preventing detachment specifically during microtubule assembly, Stu2 enables long-lived kinetochore attachments, especially when tension is high. Conversely, by promoting detachment during disassembly at low force, Stu2 helps to ensure that relaxed kinetochore attachments are short-lived. Both of these effects together result in the selective stabilization of tension-bearing attachments. In the future, it will be critical to learn how tension regulates these Stu2 activities and how the intrinsic tension sensitivity that they create is integrated with the error correction activity of Aurora B. It will also be important

to determine how these activities change at anaphase, where kinetochores stay attached to disassembling tips at low tension. Our observation that removing Stu2 function from kinetochores dramatically improves the attachment duration on disassembling microtubules suggests that Stu2 may be inhibited or released at anaphase onset to maintain kinetochore attachments during prolonged microtubule disassembly. Intriguingly, Stu2 family members exhibit regulated changes in localization during the cell cycle that are required for accurate chromosome segregation (Aoki et al., 2006; Aravamudhan et al., 2014).

Conclusions

Our findings reveal an uncharacterized function of Stu2 that is regulated mechanically, such that kinetochore-microtubule attachments are intrinsically stabilized by tension, implicating it in the correction of erroneous kinetochore-microtubule attachments. Stu2's association with kinetochores and its ability to strengthen kinetochore-tip attachments are properties shared by its human ortholog, ch-TOG. Chromosome segregation errors are the most prevalent genetic alteration in tumor cells and have been proposed to be a major factor in the evolution of cancer (reviewed in Gordon et al., 2012). Because ch-TOG is overexpressed in various tumor types (named for colonic and hepatic tumor overexpressed gene; Charrasse et al., 1995, 1998), it will be important to determine whether its function at kinetochores

contributes to tumorigenesis and, ultimately, whether kinetochore-associated ch-TOG might be a useful therapeutic target.

EXPERIMENTAL PROCEDURES

Strain Construction and Microbial Techniques

Standard media and microbial techniques were used (Sherman et al., 1974). Yeast strains were constructed by standard genetic techniques. Specific plasmid construction and yeast strains used in this study are described in Supplemental Experimental Procedures and Table S1. The auxin inducible degron (AID) system was used as described in Nishimura et al. (2009). 100–500 μM IAA (indole-3-acetic acid; auxin) was added to media to induce degradation of the AID-tagged protein. To monitor chromosome segregation, cells carrying a tandem array of lacO sequences integrated at *TRP1* (~12 kb from CENIV) and a LacI-GFP fusion (Straight et al., 1996) were arrested in G1 with α-factor. Cells were released into medium containing auxin, lacking α-factor pheromone, and chromosome segregation was determined in binucleate cells. To examine kinetochore localization and spindle morphology, exponentially growing cultures were treated with auxin for 2.5 hr, fixed, and analyzed for Mtw1-3GFP localization and Tub1-CFP spindle morphology. Cells were imaged using a Nikon E600 microscope with a 60× objective (NA = 1.40), equipped with a Photometrics Cascade 512B digital camera. Seven z stacks (0.2 μm apart) were acquired and all frames with nuclear signal in focus were maximally projected. See Supplemental Experimental Procedures for further details.

Protein Biochemistry

Native kinetochore particles, Ndc80c, and Stu2 were purified from asynchronously growing *S. cerevisiae* cells as in Akiyoshi et al. (2010) or as described in Supplemental Experimental Procedures. Standard procedures for SDS-PAGE and immunoblotting were followed. For in vitro binding assays, purified native Ndc80c or kinetochores were immobilized and incubated with 30–90 ng of purified Stu2-3V5 for 30 min at room temperature with gentile agitation. Associated proteins were eluted by peptide elution and analyzed by silver stained SDS-PAGE or immunoblotting. Immobilized GFP-tagged ch-TOG was incubated with 100 nM of Hec1/Ndc80c (prepared as in Umbreit et al., 2012) for 40 min at room temperature with gentile agitation. Associated proteins were eluted by boiling in sample buffer and analyzed by immunoblotting. For more details, see Supplemental Experimental Procedures.

Optical Trap Assays

Optical-trap-based bead motility assays were performed as in Akiyoshi et al. (2010) and Umbreit et al. (2012). Streptavidin-coated beads were functionalized with biotinylated anti-penta-His antibody and decorated with purified kinetochores (via Dsn1-6His-3Flag), purified native Ndc80 complex (via Spc24-6His-3Flag), purified Hec1/Ndc80 complex (via Spc24-6His), or purified native Stu2 (via Stu2-6His-3Flag). Protein-coated beads were bound to dynamic microtubule tips and an optical trap was used to apply a defined amount of force in the direction of microtubule assembly. See Supplemental Experimental Procedures and Tables S2 and S3 for more details.

SUPPLEMENTAL INFORMATION

Supplemental Information includes Supplemental Experimental Procedures, six figures, and three tables and can be found with this article online at http://dx.doi.org/10.1016/j.cell.2016.04.030.

AUTHOR CONTRIBUTIONS

M.P.M. conceptually designed and performed experiments, analyzed the data, and wrote the manuscript; C.L.A. and S.B. conceptually designed experiments, analyzed the data, and wrote the manuscript with M.P.M.

ACKNOWLEDGMENTS

REFERENCES

Akiyoshi, B., Sarangapani, K.K., Powers, A.F., Nelson, C.R., Reichow, S.L., Arellano-Santoyo, H., Gonen, T., Ranish, J.A., Asbury, C.L., and Biggins, S. (2010). Tension directly stabilizes reconstituted kinetochore-microtubule attachments. Nature *468*, 576–579.

Al-Bassam, J., and Chang, F. (2011). Regulation of microtubule dynamics by TOG-domain proteins XMAP215/Dis1 and CLASP. Trends Cell Biol. *21*, 604–614.

Al-Bassam, J., van Breugel, M., Harrison, S.C., and Hyman, A. (2006). Stu2p binds tubulin and undergoes an open-to-closed conformational change. J. Cell Biol. *172*, 1009–1022.

Al-Bassam, J., Kim, H., Flor-Parra, I., Lal, N., Velji, H., and Chang, F. (2012). Fission yeast Alp14 is a dose-dependent plus end-tracking microtubule polymerase. Mol. Biol. Cell *23*, 2878–2890.

Alushin, G.M., Ramey, V.H., Pasqualato, S., Ball, D.A., Grigorieff, N., Musacchio, A., and Nogales, E. (2010). The Ndc80 kinetochore complex forms oligomeric arrays along microtubules. Nature *467*, 805–810.

Aoki, K., Nakaseko, Y., Kinoshita, K., Goshima, G., and Yanagida, M. (2006). Cdc2 phosphorylation of the fission yeast Dis1 ensures accurate chromosome segregation. Curr. Biol. *16*, 1627–1635.

Aravamudhan, P., Felzer-Kim, I., Gurunathan, K., and Joglekar, A.P. (2014). Assembling the protein architecture of the budding yeast kinetochore-microtubule attachment using FRET. Curr. Biol. *24*, 1437–1446.

Ayaz, P., Ye, X., Huddleston, P., Brautigam, C.A., and Rice, L.M. (2012). A TOG:αβ-tubulin complex structure reveals conformation-based mechanisms for a microtubule polymerase. Science *337*, 857–860.

Ayaz, P., Munyoki, S., Geyer, E.A., Piedra, F.-A., Vu, E.S., Bromberg, R., Otwinowski, Z., Grishin, N.V., Brautigam, C.A., and Rice, L.M. (2014). A tethered delivery mechanism explains the catalytic action of a microtubule polymerase. eLife *3*, e03069.

Brouhard, G.J., Stear, J.H., Noetzel, T.L., Al-Bassam, J., Kinoshita, K., Harrison, S.C., Howard, J., and Hyman, A.A. (2008). XMAP215 is a processive microtubule polymerase. Cell *132*, 79–88.

Carmena, M., Wheelock, M., Funabiki, H., and Earnshaw, W.C. (2012). The chromosomal passenger complex (CPC): from easy rider to the godfather of mitosis. Nat. Rev. Mol. Cell Biol. *13*, 789–803.

Charrasse, S., Mazel, M., Taviaux, S., Berta, P., Chow, T., and Larroque, C. (1995). Characterization of the cDNA and pattern of expression of a new gene over-expressed in human hepatomas and colonic tumors. Eur. J. Biochem. *234*, 406–413.

Charrasse, S., Schroeder, M., Gauthier-Rouviere, C., Ango, F., Cassimeris, L., Gard, D.L., and Larroque, C. (1998). The TOGp protein is a new human microtubule-associated protein homologous to the *Xenopus* XMAP215. J. Cell Sci. *111*, 1371–1383.

Cheeseman, I.M. (2014). The kinetochore. Cold Spring Harb. Perspect. Biol. *6*, a015826.

Cheeseman, I.M., Brew, C., Wolyniak, M., Desai, A., Anderson, S., Muster, N., Yates, J.R., Huffaker, T.C., Drubin, D.G., and Barnes, G. (2001). Implication of a novel multiprotein Dam1p complex in outer kinetochore function. J. Cell Biol. *155*, 1137–1145.

Cheeseman, I.M., Chappie, J.S., Wilson-Kubalek, E.M., and Desai, A. (2006). The conserved KMN network constitutes the core microtubule-binding site of the kinetochore. Cell *127*, 983–997.

DeLuca, J.G., Dong, Y., Hergert, P., Strauss, J., Hickey, J.M., Salmon, E.D., and McEwen, B.F. (2005). Hec1 and Nuf2 are core components of the kinetochore outer plate essential for organizing microtubule attachment sites. Mol. Biol. Cell *16*, 519–531.

Dietz, R. (1958). [Multiple sex chromosomes in *Ostracoda cypria*, their evolution and division characteristics]. [Article in German]. Chromosoma *9*, 359–440.

Fox, J.C., Howard, A.E., Currie, J.D., Rogers, S.L., and Slep, K.C. (2014). The XMAP215 family drives microtubule polymerization using a structurally diverse TOG array. Mol. Biol. Cell *25*, 2375–2392.

Franck, A.D., Powers, A.F., Gestaut, D.R., Gonen, T., Davis, T.N., and Asbury, C.L. (2007). Tension applied through the Dam1 complex promotes microtubule elongation providing a direct mechanism for length control in mitosis. Nat. Cell Biol. *9*, 832–837.

Franck, A.D., Powers, A.F., Gestaut, D.R., Davis, T.N., and Asbury, C.L. (2010). Direct physical study of kinetochore-microtubule interactions by reconstitution and interrogation with an optical force clamp. Methods *51*, 242–250.

Gandhi, S.R., Gierliński, M., Mino, A., Tanaka, K., Kitamura, E., Clayton, L., and Tanaka, T.U. (2011). Kinetochore-dependent microtubule rescue ensures their efficient and sustained interactions in early mitosis. Dev. Cell *21*, 920–933.

Gard, D.L., and Kirschner, M.W. (1987). Microtubule assembly in cytoplasmic extracts of *Xenopus* oocytes and eggs. J. Cell Biol. *105*, 2191–2201.

Gergely, F., Draviam, V.M., and Raff, J.W. (2003). The ch-TOG/XMAP215 protein is essential for spindle pole organization in human somatic cells. Genes Dev. *17*, 336–341.

Gillett, E.S., Espelin, C.W., and Sorger, P.K. (2004). Spindle checkpoint proteins and chromosome-microtubule attachment in budding yeast. J. Cell Biol. *164*, 535–546.

Gordon, D.J., Resio, B., and Pellman, D. (2012). Causes and consequences of aneuploidy in cancer. Nat. Rev. Genet. *13*, 189–203.

Goshima, G., and Yanagida, M. (2000). Establishing biorientation occurs with precocious separation of the sister kinetochores, but not the arms, in the early spindle of budding yeast. Cell *100*, 619–633.

Hanisch, A., Silljé, H.H.W., and Nigg, E.A. (2006). Timely anaphase onset requires a novel spindle and kinetochore complex comprising Ska1 and Ska2. EMBO J. *25*, 5504–5515.

He, X., Asthana, S., and Sorger, P.K. (2000). Transient sister chromatid separation and elastic deformation of chromosomes during mitosis in budding yeast. Cell *101*, 763–775.

He, X., Rines, D.R., Espelin, C.W., and Sorger, P.K. (2001). Molecular analysis of kinetochore-microtubule attachment in budding yeast. Cell *106*, 195–206.

Hsu, K.-S., and Toda, T. (2011). Ndc80 internal loop interacts with Dis1/TOG to ensure proper kinetochore-spindle attachment in fission yeast. Curr. Biol. *21*, 214–220.

Kalantzaki, M., Kitamura, E., Zhang, T., Mino, A., Novák, B., and Tanaka, T.U. (2015). Kinetochore-microtubule error correction is driven by differentially regulated interaction modes. Nat. Cell Biol. *17*, 421–433.

Kitamura, E., Tanaka, K., Komoto, S., Kitamura, Y., Antony, C., and Tanaka, T.U. (2010). Kinetochores generate microtubules with distal plus ends: their roles and limited lifetime in mitosis. Dev. Cell *18*, 248–259.

Kosco, K.A., Pearson, C.G., Maddox, P.S., Wang, P.J., Adams, I.R., Salmon, E.D., Bloom, K., and Huffaker, T.C. (2001). Control of microtubule dynamics by Stu2p is essential for spindle orientation and metaphase chromosome alignment in yeast. Mol. Biol. Cell *12*, 2870–2880.

Krenn, V., and Musacchio, A. (2015). The Aurora B Kinase in Chromosome Bi-Orientation and Spindle Checkpoint Signaling. Front. Oncol. *5*, 225.

Ma, L., McQueen, J., Cuschieri, L., Vogel, J., and Measday, V. (2007). Spc24 and Stu2 promote spindle integrity when DNA replication is stalled. Mol. Biol. Cell *18*, 2805–2816.

Marco, E., Dorn, J.F., Hsu, P.H., Jaqaman, K., Sorger, P.K., and Danuser, G. (2013). *S. cerevisiae* chromosomes biorient via gradual resolution of syntely between S phase and anaphase. Cell *154*, 1127–1139.

Maure, J.-F., Komoto, S., Oku, Y., Mino, A., Pasqualato, S., Natsume, K., Clayton, L., Musacchio, A., and Tanaka, T.U. (2011). The Ndc80 loop region facilitates formation of kinetochore attachment to the dynamic microtubule plus end. Curr. Biol. *21*, 207–213.

McCleland, M.L., Kallio, M.J., Barrett-Wilt, G.A., Kestner, C.A., Shabanowitz, J., Hunt, D.F., Gorbsky, G.J., and Stukenberg, P.T. (2004). The vertebrate Ndc80 complex contains Spc24 and Spc25 homologs, which are required to establish and maintain kinetochore-microtubule attachment. Curr. Biol. *14*, 131–137.

Meraldi, P., Draviam, V.M., and Sorger, P.K. (2004). Timing and checkpoints in the regulation of mitotic progression. Dev. Cell *7*, 45–60.

Mitchison, T., and Kirschner, M. (1984). Dynamic instability of microtubule growth. Nature *312*, 237–242.

Nicklas, R.B., and Koch, C.A. (1969). Chromosome micromanipulation. 3. Spindle fiber tension and the reorientation of mal-oriented chromosomes. J. Cell Biol. *43*, 40–50.

Nishimura, K., Fukagawa, T., Takisawa, H., Kakimoto, T., and Kanemaki, M. (2009). An auxin-based degron system for the rapid depletion of proteins in nonplant cells. Nat. Methods *6*, 917–922.

Nogales, E., and Ramey, V.H. (2009). Structure-function insights into the yeast Dam1 kinetochore complex. J. Cell Sci. *122*, 3831–3836.

Ohkura, H., Adachi, Y., Kinoshita, N., Niwa, O., Toda, T., and Yanagida, M. (1988). Cold-sensitive and caffeine-supersensitive mutants of the *Schizosaccharomyces pombe dis* genes implicated in sister chromatid separation during mitosis. EMBO J. *7*, 1465–1473.

Pearson, C.G., Maddox, P.S., Salmon, E.D., and Bloom, K. (2001). Budding yeast chromosome structure and dynamics during mitosis. J. Cell Biol. *152*, 1255–1266.

Pearson, C.G., Maddox, P.S., Zarzar, T.R., Salmon, E.D., and Bloom, K. (2003). Yeast kinetochores do not stabilize Stu2p-dependent spindle microtubule dynamics. Mol. Biol. Cell *14*, 4181–4195.

Podolski, M., Mahamdeh, M., and Howard, J. (2014). Stu2, the budding yeast XMAP215/Dis1 homolog, promotes assembly of yeast microtubules by increasing growth rate and decreasing catastrophe frequency. J. Biol. Chem. *289*, 28087–28093.

Powers, A.F., Franck, A.D., Gestaut, D.R., Cooper, J., Gracyzk, B., Wei, R.R., Wordeman, L., Davis, T.N., and Asbury, C.L. (2009). The Ndc80 kinetochore complex forms load-bearing attachments to dynamic microtubule tips via biased diffusion. Cell *136*, 865–875.

Severin, F., Habermann, B., Huffaker, T., and Hyman, T. (2001). Stu2 promotes mitotic spindle elongation in anaphase. J. Cell Biol. *153*, 435–442.

Sherman, F., Fink, G., and Lawrence, C. (1974). Methods in Yeast Genetics (Cold Spring Harbor, New York: Cold Spring Harbor Laboratory Press).

Shirasu-Hiza, M., Coughlin, P., and Mitchison, T. (2003). Identification of XMAP215 as a microtubule-destabilizing factor in *Xenopus* egg extract by biochemical purification. J. Cell Biol. *161*, 349–358.

Straight, A.F., Belmont, A.S., Robinett, C.C., and Murray, A.W. (1996). GFP tagging of budding yeast chromosomes reveals that protein-protein interactions can mediate sister chromatid cohesion. Curr. Biol. *6*, 1599–1608.

Tanaka, K., Mukae, N., Dewar, H., van Breugel, M., James, E.K., Prescott, A.R., Antony, C., and Tanaka, T.U. (2005). Molecular mechanisms of kinetochore capture by spindle microtubules. Nature *434*, 987–994.

Tang, N.H., Takada, H., Hsu, K.-S., and Toda, T. (2013). The internal loop of fission yeast Ndc80 binds Alp7/TACC-Alp14/TOG and ensures proper chromosome attachment. Mol. Biol. Cell *24*, 1122–1133.

Trushko, A., Schäffer, E., and Howard, J. (2013). The growth speed of microtubules with XMAP215-coated beads coupled to their ends is increased by tensile force. Proc. Natl. Acad. Sci. USA *110*, 14670–14675.

Umbreit, N.T., Gestaut, D.R., Tien, J.F., Vollmar, B.S., Gonen, T., Asbury, C.L., and Davis, T.N. (2012). The Ndc80 kinetochore complex directly modulates microtubule dynamics. Proc. Natl. Acad. Sci. USA *109*, 16113–16118.

van Breugel, M., Drechsel, D., and Hyman, A. (2003). Stu2p, the budding yeast member of the conserved Dis1/XMAP215 family of microtubule-associated proteins is a plus end-binding microtubule destabilizer. J. Cell Biol. *161*, 359–369.

Wang, P.J., and Huffaker, T.C. (1997). Stu2p: A microtubule-binding protein that is an essential component of the yeast spindle pole body. J. Cell Biol. *139*, 1271–1280.

Welburn, J.P.I., Grishchuk, E.L., Backer, C.B., Wilson-Kubalek, E.M., Yates, J.R., 3rd, and Cheeseman, I.M. (2009). The human kinetochore Ska1 complex facilitates microtubule depolymerization-coupled motility. Dev. Cell *16*, 374–385.

Widlund, P.O., Stear, J.H., Pozniakovsky, A., Zanic, M., Reber, S., Brouhard, G.J., Hyman, A.A., and Howard, J. (2011). XMAP215 polymerase activity is built by combining multiple tubulin-binding TOG domains and a basic lattice-binding region. Proc. Natl. Acad. Sci. USA *108*, 2741–2746.

Wigge, P.A., and Kilmartin, J.V. (2001). The Ndc80p complex from *Saccharomyces cerevisiae* contains conserved centromere components and has a function in chromosome segregation. J. Cell Biol. *152*, 349–360.
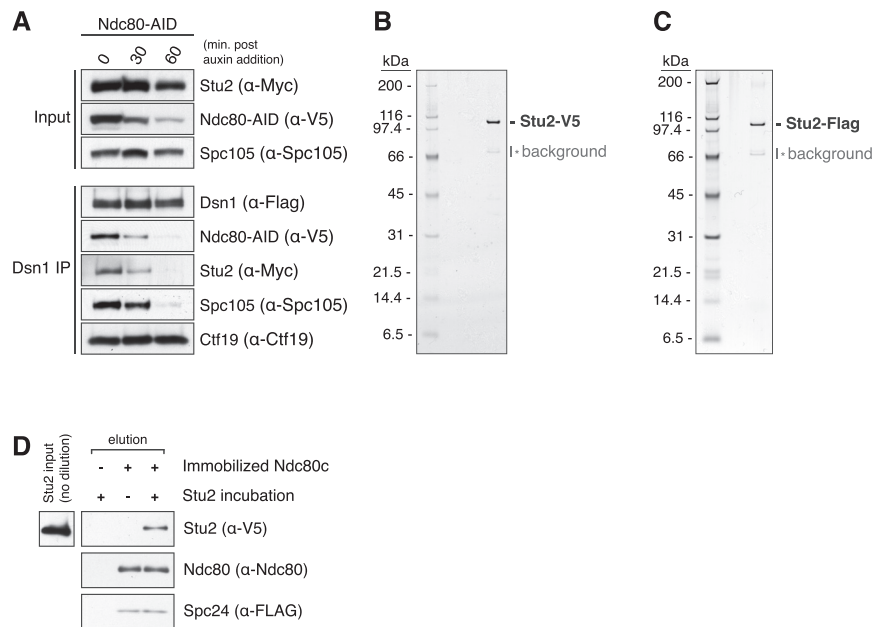
Figure S1. Characterization of Stu2 Binding to Kinetochores, Related to Figure 1

(A) Exponentially growing Ndc80-AID cultures that also contained Dsn1-6His-3Flag and Stu2-13Myc (SBY11855) were treated with 500 μM auxin. Protein lysates were prepared 0, 30, or 60 min post auxin addition and kinetochore particles were purified by α-Flag IP and analyzed by immunoblotting with α-Flag, α-V5, α-Myc, α-Spc105 and α-Ctf19 antibodies.

(B) Protein lysates were prepared from exponentially growing cultures containing Stu2-3V5 (SBY11709). Stu2-3V5 was purified by α-V5 IP, followed by washes in buffer containing 1.0 M KCl (BH 1.0) then V5 peptide elution. Eluate was run on an SDS-PAGE gel and analyzed by silver stain. Background bands were determined by mass spectrometry to be the highly homologous heat shock proteins Ssa1, Ssa2 (70 kDa), and Ssb1, Ssb2 (66 kDa), which are common co-purifying proteins in IPs from yeast lysates (Cheeseman et al., 2002), and were isolated in all purifications.

(C) Protein lysates were prepared from exponentially growing cultures containing Stu2-3Flag (SBY12275). Stu2-3Flag was purified by α-Flag IP, followed by washes in buffer containing 1.0 M KCl (BH 1.0) then Flag peptide elution. Eluate was run on an SDS-PAGE gel and analyzed by silver stain.

(D) Samples from Figure 1C were analyzed by immunoblotting with α-Flag, α-V5 and α-Ndc80 antibodies.
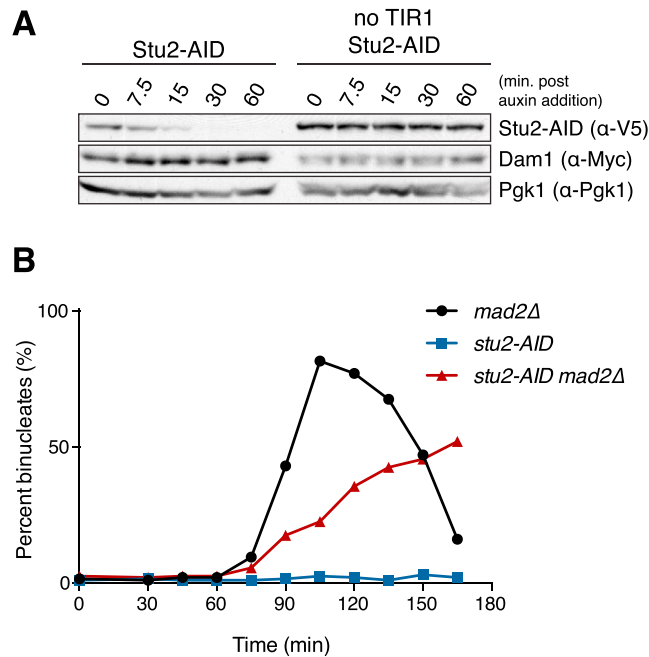
Figure S2. Stu2-AID Protein Is Rapidly Degraded and Induces a Spindle Checkpoint-Dependent Metaphase Arrest, Related to Figure 2

(A) Whole cell lysate protein samples from cultures described in Figure 3B were prepared and analyzed by immunoblotting with α-V5 (Stu2-AID), α-Myc (Dam1-9Myc) and α-Pgk1 antibodies. Pgk1 was used as a loading control.

(B) Exponentially growing *mad2Δ* (black; SBY468), *stu2-AID* (blue; SBY16239) or *mad2Δ stu2-AID* (red; SBY16236) cells containing fluorescently labeled chromosome IV were arrested in G1 with α-factor then released from arrest to undergo cell division in the presence of 500 μM auxin. Cell-cycle progression was determined by quantifying the number of cells with either a single DAPI-stained DNA mass (mononucleate) or two DNA masses (binucleate). Shown is the accumulation of binucleate cells for each from a representative experiment; n = 200 cells per time point.
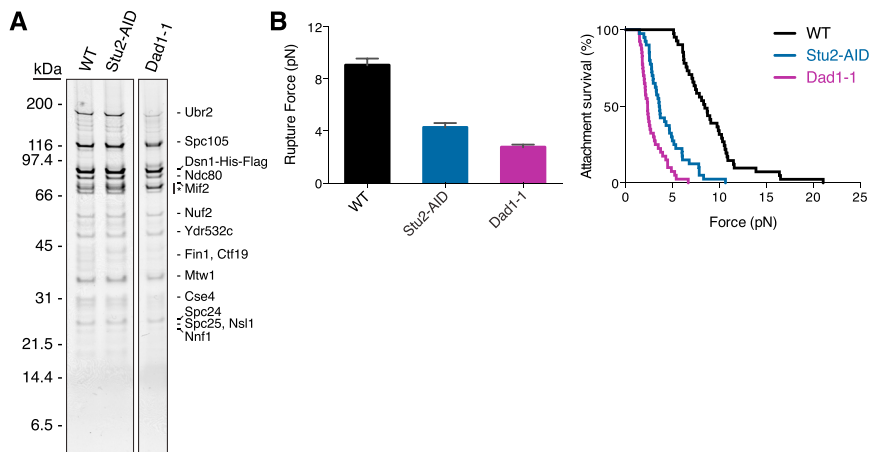
Figure S3. Kinetochore-Associated Stu2 Significantly Contributes to the Overall Attachment Strength of Purified Kinetochore Particles, Related to Figure 3

(A) Kinetochore particles were purified by α-Flag IP and analyzed by SDS-PAGE and silver stain analysis. Protein lysate was prepared from a culture shifted to 37°C (for 2 hr) containing Dsn1-6His-3Flag and the temperature sensitive *dad1-1* allele ('Dad1-1'; SBY8944). Samples from Figure 3A shown for comparison.

(B) Left: mean rupture forces for wild-type, Stu2-AID and Dad1-1 kinetochore particles. Untreated wild-type and Stu2-AID data are shown from Figure 3E for comparison. Error bars represent SEM (n = 40–41 events). Right: attachment survival versus force for the same data.
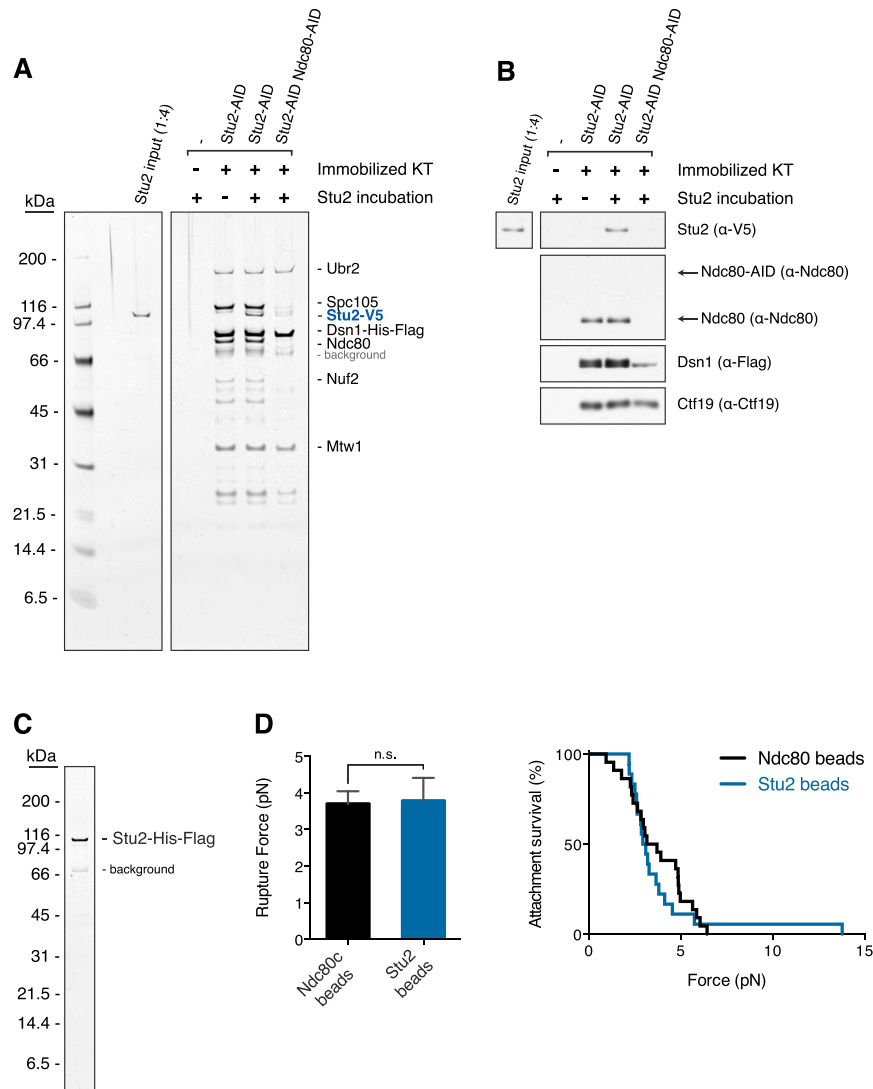
Figure S4. Stu2 Binds to Purified Kinetochores and Alone Can Bind to Dynamic Microtubule Tips, Related to Figure 3

(A) Protein lysates were prepared from exponentially growing cultures containing Dsn1-6His-3Flag Stu2-AID (SBY13772) or Dsn1-6His-3Flag Stu2-AID Ndc80-AID (SBY14584) treated with 500 μM auxin for 30 min prior to harvesting cells or from an untagged strain (SBY3). Kinetochore particles were immobilized by α-Flag IP, control beads lacking kinetochore particles were incubated with untagged lysate (from SBY3). Control or immobilized kinetochore-beads were incubated with 30 ng of Stu2-3V5 (purified as in part C) for 30 min at room temperature, washed, and eluted with Flag peptide. Kinetochore-bound proteins were analyzed by silver stained SDS-PAGE.

(B) Samples from (A) were analyzed by immunoblotting with α-Flag, α-V5, α-Ndc80 and α-Ctf19 antibodies.

(C) Protein lysate was prepared from an exponentially growing culture containing Stu2-6His-3Flag (SBY13095). Stu2-6His-3Flag was purified by α-Flag IP, followed by washes in buffer containing 1.0 M KCl (BH 1.0) then Flag peptide elution. Eluate was run on an SDS-PAGE gel and analyzed by silver stain.

(D) Left: mean rupture forces for Ndc80c- and Stu2-based couplers. Error bars represent SEM (n = 18–22 events). p value determined using a two-tailed unpaired t test (n.s. = not significant). Right: attachment survival probability versus force for the same data. Data for Ndc80c-based couplers are from Figure 3F and shown for comparison.
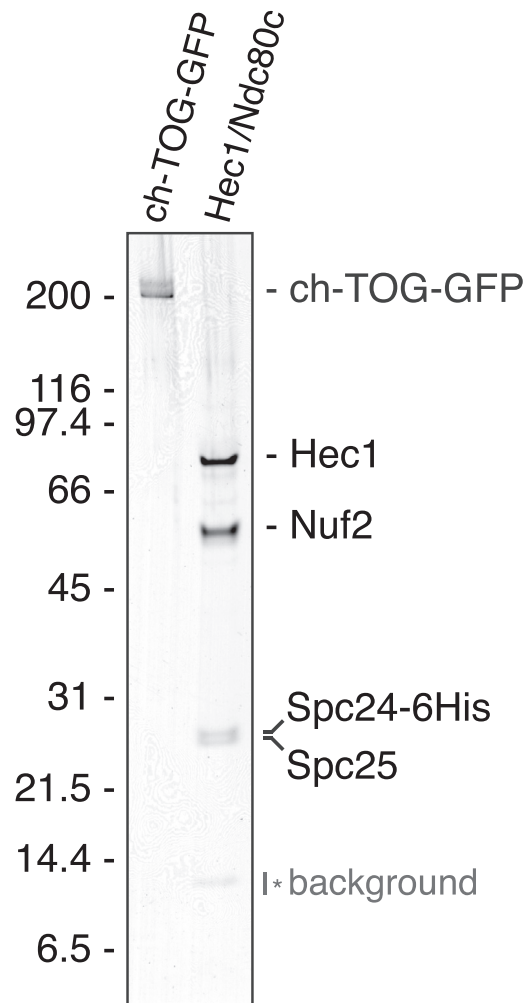
Figure S5. Purified Hec1/Ndc80c and ch-TOG, Related to Figure 4

35 ng and 30 ng of recombinant Hec1/Ndc80c or ch-TOG, respectively, run on an SDS-PAGE gel and silver stained.
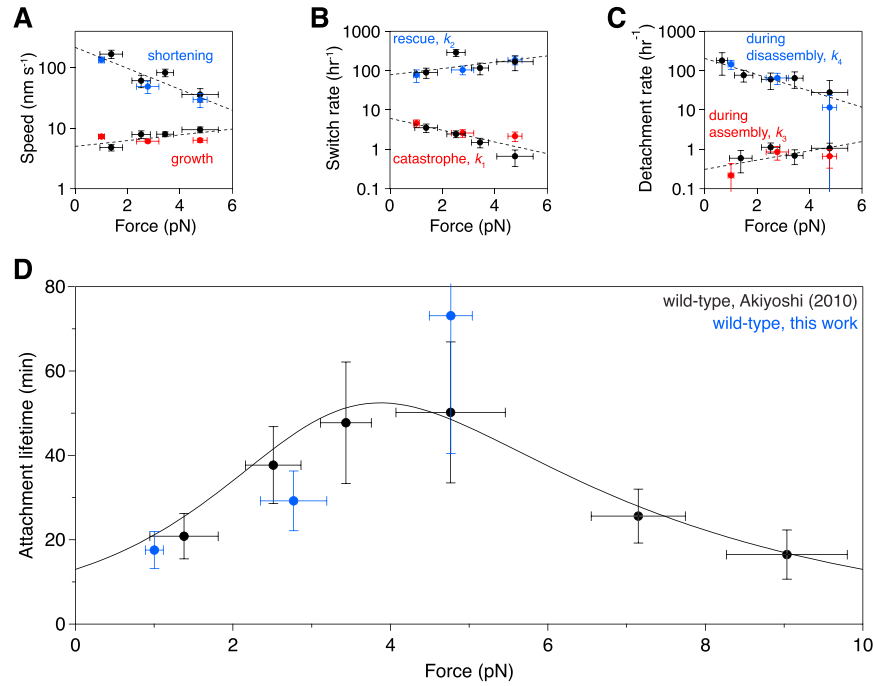
Figure S6. Comparison of Wild-Type Kinetochore Particles, Related to Figure 5.

(A–D) Rates of microtubule assembly (growth) and disassembly (shortening) (A), microtubule catastrophe, k_1 and rescue, k_2 (B), kinetochore detachment during microtubule assembly, k_3, kinetochore detachment during microtubule disassembly, k_4 (C), and kinetochore attachment lifetime (D) determined for newly measured wild-type particles (red or blue) subjected continuously to indicated amounts of force. The same measurements are shown from Akiyoshi et al. (2010; black) for comparison. The newly measured wild-type data were combined with wild-type data from Akiyoshi et al. (2010) to calculate the rates displayed in Figures 5 and 6. The exponential fits shown in (A)–(C) are for the combined wild-type data, as also shown in Figures 5 and 6. The curve in (D) shows prediction of the two-state model for the combined wild-type data (see text), as also shown in Figure 6. The error bars in (A)–(C) represent uncertainty due to counting statistics (n = 4–92 events).

Supplemental Information

A TOG Protein Confers Tension Sensitivity to

Kinetochore-Microtubule Attachments

Matthew P. Miller, Charles L. Asbury, and Sue Biggins

Supplemental Experimental Procedures

Strain Construction and Microbial Techniques

Strain Construction
Saccharomyces cerevisiae strains used in this study are described in Table S1 and are derivatives of SBY3 (W303). *DSN1-6His-3Flag* is described in (Akiyoshi et al., 2010). *MTW1-3GFP* and *TUB1-CFP* are described in (Pinsky et al., 2006). *STU2-13Myc*, *STU2-3V5*, *STU2-3Flag*, *SPC24-6His-3Flag*, *STU2-6His-3Flag*, *ndc80-3V5-IAA7*, *ndc80-3V5-IAA17*, *stu2-3V5-IAA7*, *stu2-3HA-IAA7*, *spc105-3HA-IAA7* and *DAM1-9Myc* were constructed by PCR-based methods described in (Longtine et al., 1998), integrated at the endogenous loci and are fully functional. A strain containing a *cdc20-IAA17* allele was kindly provided by Eris Duro and Adèle Marston. *pADH1-TIR1-9Myc* is described in (Nishimura et al., 2009). *pGPD1-TIR1* integration plasmids (pSB2271 for integration at *LEU2*, pSB2273 for integration at *HIS3* or pSB2275 for integration at *TRP1*) as well as 3V5-IAA7 and 3V5-IAA17 tagging plasmids (pSB2065 and pSB2067, respectively) were provided by Leon Chan. A 3HA-IAA7 tagging plasmid (pSB2229) was constructed by cloning a PCR product containing 3HA flanked by PacI and XhoI restriction sites into the PacI and XhoI sites of pSB2065. A *pSTU2-STU2-3V5* PCR product containing PspOMI/XhoI restriction sites was amplified from genomic DNA of a *STU2-3V5* strain (described above), cloned into the same restriction sites of integration plasmid pSB2223 (generating pSB2232), and cut with SwaI to integrate at the *LEU2* locus.

Auxin Inducible Degradation
The auxin inducible degron (AID) system was used essentially as described (Nishimura et al., 2009). Briefly, cells expressed C-terminal fusions of the protein of interest to an auxin responsive protein (IAA7 or IAA17) at the endogenous locus. Cells also expressed TIR1, which is required for auxin-induced degradation. 100-500 μM IAA (indole-3-acetic acid dissolved in DMSO; Sigma) was added to media to induce degradation of the AID-tagged protein. Auxin was added for 30 min prior to harvesting cells or as is indicated in figure legends.

Chromosome Segregation Assay
Cells were grown in yeast peptone dextrose rich (YPD) medium. Exponentially growing *MATa mad2Δ*, *stu2-AID* or *stu2-AID mad2Δ* cells also carrying a tandem array of lacO sequences integrated at *TRP1* (~12kb from CENIV) and a LacI-GFP fusion (Straight et al., 1996) were arrested in G1 with 1μg/ml α-factor. When arrest was complete, cells were released into medium lacking α-factor pheromone and containing 500μM IAA. ~75 min after G1 release, 1μg/ml α-factor was added to prevent a second cell division. Samples were taken every 15min after G1 release to determine chromosome segregation in anaphase (For Figure 2E, chromosome segregation at 135 min post-release is quantified).

Cell Fixation and Imaging Conditions
Exponentially growing cultures were treated with 500 μM auxin for 2.5h, then fixed (see below) and analyzed for Mtw1-3GFP localization and spindle morphology (Tub1-CFP). An aliquot of cells was fixed with 3.7% formaldehyde in 100mM phosphate buffer (pH 6.4) for 5 min. Cells were washed once with 100mM phosphate (pH 6.4), resuspended in 100mM phosphate, 1.2M sorbitol buffer (pH 7.5) and permeabilized with 1% Triton X-100 stained with 1 μg/ml DAPI (4', 6-diamidino-2-phenylindole; Molecular Probes). Cells were imaged using a Nikon E600 microscope with a 60X objective (NA=1.40), equipped with a Photometrics Cascade 512B digital camera. Seven Z-stacks (0.2 micron apart) were acquired and all frames with nuclear signal in focus were maximally projected. NIS Elements software (Nikon) was used for image acquisition and processing.

Spotting Assay
For the spotting assay, the desired strains were grown overnight in YPD medium. The following day, cells were diluted to OD$_{600}$ ~1.0 from which a serial 1:5 dilution series was made and spotted on YPD+DMSO or YPD+100 μM IAA (indole-3-acetic acid dissolved in DMSO) plates. Plates were incubated at 23°C for 3 days.

Protein Biochemistry

Purification of Native Kinetochore Particles, Ndc80 Complex and Stu2
Native kinetochore particles, Ndc80 complex and Stu2 were purified from asynchronously growing *S. cerevisiae* cells as described below (unless otherwise noted in the text). For kinetochore particles, an α-Flag immunoprecipitation of Dsn1-6His-3Flag was performed (essentially as described in Akiyoshi et al., 2010). To purify the Ndc80c, an α-Flag immunoprecipitation of Spc24-6His-3Flag was performed. To purify Stu2, an α-Flag immunoprecipitation of Stu2-3Flag or Stu2-6His-3Flag or an α-V5 immunoprecipitation of Stu2-3V5 was performed. For each, cells were grown in yeast peptone dextrose rich (YPD) medium. For strains containing Stu2-AID, Spc105-AID and/or Ndc80-AID, cells were treated with 500 μM auxin 30 min prior to harvesting. Protein lysates were prepared by lysing cells either in a blender in the presence of dry ice (as described in Akiyoshi et al., 2010), in a Freezer/Mill (SPEX SamplePrep) submerged in liquid nitrogen (Sarangapani et al., 2014) or mechanically disrupted in the presence of lysis buffer using glass beads and a beadbeater (Biospec Products). Lysed cells were resuspended in buffer H (BH) (25 mM HEPES pH 8.0, 2 mM $MgCl_2$, 0.1 mM EDTA, 0.5 mM EGTA, 0.1% NP-40, 15% glycerol with 150 mM KCl for native kinetochores, 750 mM KCl for native Ndc80 complex or 1 M KCl for native Stu2) containing protease inhibitors (at 20 μg mL^{-1} final concentration for each of leupeptin, pepstatin A, chymostatin and 200 μM phenylmethylsulfonyl fluoride) and phosphatase inhibitors (0.1 mM Na-orthovanadate, 0.2 μM microcystin, 2 mM β-glycerophosphate, 1 mM Na pyrophosphate,5 mM NaF) followed by ultracentrifugation at 98,500 g for 90 min at 4 °C. Lysates prepared using the beadbeater were instead centrifuged at 16,100 g for 30 min at 4 °C. Dynabeads conjugated with α-Flag or α-V5 antibodies were incubated with extract for 3 h with constant rotation, followed by three washes with BH containing protease inhibitors, phosphatase inhibitors, 2 mM dithiothreitol (DTT) and either 150 mM KCl (kinetochores) or 1 M KCl (Ndc80 complex and Stu2). Beads were further washed twice with BH containing 150 mM KCl and protease inhibitors. Associated proteins were eluted from the beads by gentle agitation of beads in elution buffer (0.5 mg ml^{-1} 3Flag peptide or 0.5 mg ml^{-1} 3V5 peptide in BH with 150 mM KCl and protease inhibitors) for 30 min at room temperature. To eliminate the co-purification of the Spc105 complex with the native Ndc80 complex, we immunoprecipitated Spc24-6His-3Flag from cells carrying an *spc105-AID* allele that were treated with 500 μM auxin for 30 min.

Immunoblot Analysis
For immunoblot analysis, cell lysates were prepared as described above (Protein biochemistry section) or by pulverizing cells with glass beads in sodium dodecyl sulfate (SDS) buffer using a bead-beater (Biospec Products). Standard procedures for sodium dodecyl sulfate-polyacrylamide gel electrophoresis (SDS-PAGE) and immunoblotting were followed as described in (Burnette, 1981; Towbin et al., 1992). A nitrocellulose membrane (BioRad) was used to transfer proteins from polyacrylamide gels. Commercial antibodies used for immunoblotting were as follows: α-Myc, 9E10 (Covance) at a 1:10,000 dilution; α-Flag, M2 (Sigma-Aldrich) 1:3,000; α-V5 (Invitrogen) 1:5,000; α-HA, 12CA5 (Roche) 1:10,000; α-GFP, JL-8 (Living Colors) 1:5,000; α-Pgk1 (Invitrogen) 1:10,000; α-Hec1, 9G3 (Abcam) 1:1,000. α-Spc105 antibodies were used at 1:10,000 (Akiyoshi et al., 2010); Antibodies to Ctf19, and Ndc80 were kind gifts from Arshad Desai and were used at: α-Ctf19, (OD10) 1:1,000; and α-Ndc80, (OD4) 1:10,000. The secondary antibodies used were a sheep anti-mouse antibody conjugated to horseradish peroxidase (HRP) (GE Biosciences) at a 1:10,000 dilution or a donkey anti-rabbit antibody conjugated to HRP (GE Biosciences) at a 1:10,000 dilution. Antibodies were detected using the SuperSignal West Dura Chemiluminescent Substrate (Thermo Scientific).

In Vitro Binding Assays
To examine the binding of Stu2 to the Ndc80c or to purified kinetochores, Stu2-3V5 and native Ndc80c or kinetochores were purified from exponentially growing yeast cells as described above (Protein biochemistry section). Prior to eluting purified Ndc80c or kinetochores from α-Flag dynabeads, beads were incubated with 15 μl (30-90 ng) of purified Stu2-3V5 for 30 min at room temperature with gentile agitation. Beads were then washed twice with BH containing 150 mM KCl and protease inhibitors. Associated proteins were eluted from the beads by gentle agitation of beads in elution buffer (0.5 mg ml^{-1} 3Flag peptide in BH with 150 mM KCl and protease inhibitors) for 30 min at room temperature.

To examine the binding of ch-TOG to the Hec1/Ndc80c, GFP-tagged ch-TOG was immobilized by α-GFP IP. Immobilized ch-TOG-beads were incubated with 100 nM of Hec1/Ndc80c (prepared as in

Umbreit et al., 2012) for 40 min at room temperature with gentile agitation. Beads were then washed twice with BH containing 150 mM KCl and protease inhibitors. Associated proteins were eluted by boiling in sample buffer. ch-TOG-bound proteins were analyzed by immunoblotting with α-GFP and α-Hec1 antibodies.

Recombinant ch-TOG Expression and Purification

A sequence encoding PreScission protease site and EGFP was fused to the 3' end of the cDNA encoding human ch-TOG (Genebank: BC120869). For affinity purification, a sequence encoding a Tobacco Etch Virus (TEV) protease site and hexahistidin-tag was fused to the 3'end of the EGFP sequence. The sequence encoding chTOG-PreScission-EGFP-TEV-6His was then cloned into NcoI/HindIII site of a pFastBac-HtB vector. The Bac-to-Bac system (Life Technologies) was used to generate recombinant baculovirus. HiveFive cells (Life Technologies), grown to 3.0-3.5 cells/ml in Sf-900 II SFM (Life Technologies 10902-096) supplemented with 1X Antibiotic-Antimyocotic (Life Technologies 15240-062), were infected with P3 viral stocks at a multiplicity of infection (MOI) of 50. Cells were cultured in suspension at 27 °C and harvested at 60 hours after infection. The following steps were done on ice or at 4 °C. We lysed cells in an equal volume of lysis buffer (50 mM K-Phosphate, 20 mM Imidazole, 400 mM KCl, 2 mM MgCl$_2$, 5% glycerol, 0.005% Brij-35, 2 mM TCEP, 3 U/ml benzonase, 4 mM Benzamidine HCl, 1 mM PMSF 1X protease inhibitor Roche Complete EDTA-free, pH 7.2) by dounce homogenizer (20 strokes) and centrifuged the homogenate at 55,000 rpm in a Ti70 rotor (Beckman Coulter) for 1 hr. The supernatant was incubated with Ni-NTA resin for 40 min. Ni-NTA resin with ch-TOG-GFP was washed with wash buffer 1 (50 mM K-Phosphate, 20 mM Imidazole, 400 mM KCl, 2 mM MgCl$_2$, 10% glycerol, 0.005% Brij-35 and 2 mM TCEP, pH 8.0) and wash buffer 2 (50 mM K-Phosphate, 60 mM Imidazole, 400 mM KCl, 2 mM MgCl$_2$, 5% glycerol, 0.005% Brij-35 and 2 mM TCEP, pH 8.0). ch-TOG-GFP was eluted with elution buffer (50 mM K-Phosphate, 400 mM Imidazole, 150 mM KCl, 2 mM MgCl$_2$, 10% glycerol, 0.005% Brij-35 and 5 mM β-ME, pH 8.0) and then gel filtered through a Superdex 200 16/60 column. Fractions containing ch-TOG-GFP were pooled, digested with TEV, and dialyzed against 500 mL TEV digestion buffer (50 mM K-Phosphate, 20 mM imidazole, 2 mM MgCl$_2$, 400 mM KCl, 10% glycerol and 5 mM β-ME, pH 8.0) at 4 °C overnight. The next day, the digested protein was flowed through 1 mL HisTrap HP column (GE Life Sciences 17-5247-01) and gel filtered through a Superose 6 10/300 GL column equilibrated in TEV digestion buffer. Fractions containing ch-TOG-GFP were pooled and dialyzed against 500 mL storage buffer (50 mM K-Phosphate, 2 mM MgCl$_2$, 400 mM KCl, 10% glycerol and 5 mM β-ME, pH 8.0) at 4°C for 6 hr. Protein aliquots were snap frozen in liquid nitrogen.

Optical Trap Assays

Bead Preparation for Optical Trap Assays

Optical trap-based bead motility assays were performed as in (Akiyoshi et al., 2010; Umbreit et al., 2012). Streptavidin-coated 0.44-μm polystyrene beads (Spherotech) were functionalized with biotinylated anti-penta-His antibody (Qiagen) and decorated with purified kinetochores (via Dsn1-6His-3Flag), purified native Ndc80 complex (via Spc24-6His-3Flag), purified Hec1/Ndc80 complex (via Spc24-6His), or purified native Stu2 (via Stu2-6His-3Flag). Bead decoration was performed in a total volume of 20 μl incubation buffer (BRB80 containing 1 mg ml^{-1} κ-casein) for kinetochores, native Ndc80c and native Stu2 or 60 μl incubation buffer (BRB80 containing 8 mg ml^{-1} BSA and 1 mM DTT) for Hec1/Ndc80c. Kinetochore particles were diluted such that the concentration of Dsn1-6His-3Flag was ~0.4 ng ul^{-1}, and then incubated with 6 pM beads for 1 h at 4 °C, as described previously (Akiyoshi et al., 2010; Sarangapani et al., 2013). Native Stu2-6His-3Flag was diluted to ~0.05 ng ul^{-1}, and then incubated with 6 pM beads for 1 h at 4 °C. 10 nM of purified native Ndc80 complex was incubated with 6 pM beads for 1 h at 4 °C, unbound protein was removed by pelleting the beads (16,000 g for 10 min at 4 °C), washing with ~200 μl of incubation buffer, pelleting beads again (16,000 g for 10 min at 4 °C) and resuspending in original volume. Beads coated with Hec1/Ndc80c were prepared in the same manner as native Ndc80 complex except that 1 nM Hec1/Ndc80c was incubated with 11 pM beads as in (Umbreit et al., 2012). For the addition of purified Stu2 to kinetochore particles, kinetochore particles (~8.4 ng of Dsn1-6His-3Flag) were incubated with ~8.4 ng of purified Stu2-3Flag for 30 min at 4 °C prior to linking the kinetochore particles to the polystyrene beads as described above. The Stu2-incubated kinetochores were diluted such that final working concentration of Stu2-Flag was 0.45 nM. For the addition of purified Stu2 to Ndc80c, Ndc80c-

decorated beads were prepared as above and purified Stu2-3V5 was added to the microtubule growth buffer (see below) to a final concentration of 2 nM. For the addition of ch-TOG to Hec1/Ndc80c, Hec1/Ndc80c-decorated beads were prepared as above and ch-TOG was added to the microtubule growth buffer to a final concentration of 10 nM.

Rupture Force Measurements

Dynamic microtubule extensions were grown from coverslip-anchored GMPCPP-stabilized microtubule seeds in a microtubule growth buffer consisting of BRB80, 1 mM GTP, 250 µg ml^{-1} glucose oxidase, 25 mM glucose, 30 µg ml^{-1} catalase, 1 mM DTT, 1.4-1.5 mg ml^{-1} purified bovine brain tubulin, and blocking protein (1 mg ml^{-1} κ-casein for the assays with kinetochores, native Ndc80c or native Stu2, and 8 mg ml^{-1} BSA for the assays with Hec1/Ndc80c). Assays were performed at 23 °C. Rupture force experiments were performed as in (Akiyoshi et al., 2010; Sarangapani et al., 2013, 2014). Briefly, an optical trap was used to apply a force of ~2-4 pN in the direction of microtubule assembly. Once beads were observed to track with microtubule growth for a distance of ~100-300 nm (to ensure end-on attachment), the applied force was increased at a constant rate of 0.25 pN s^{-1} until bead detachment. Records of bead position over time were collected and analyzed using custom software (Labview and Igor Pro, respectively) and used to determine the rupture force, which was marked as the maximum force sustained by the attachment during each event. All the individual rupture force values and calculated mean rupture strengths are provided in Table S3.

Constant Force Optical Trap Experiments

Constant force ('force-clamp') experiments were also carried out as previously described in (Akiyoshi et al., 2010; Sarangapani et al., 2013, 2014). Briefly, beads were attached to microtubule tips, and a constant force was applied continuously (in the direction of microtubule growth) throughout rounds of microtubule assembly and disassembly. Upon bead detachment, microtubule tip state was determined visually, from video-enhanced differential interference contrast (VE-DIC) images displayed live during the experiments. These video-based assessments were later confirmed during analysis of the high-resolution recordings of bead position versus time that were collected using the position sensor of the laser trap (Franck et al., 2010). Attachment lifetimes, detachment frequencies and microtubule dynamic rates were measured from the records using custom software (developed in Labview and Igor Pro).

The statistics for Stu2 depleted kinetochore particles (Figure 5C-F and Figure 6) were calculated from a set of 90 individual events, lasting a total of 18 hours, during which the kinetochores were subjected to constant tensile forces between 0.9 and 3 pN (above which their very rapid detachment prevented force clamp experiments). New statistics for wild-type kinetochore particles (Figure S6) were calculated from a set of 70 individual events, lasting a total of 19 h, under constant tensile forces between 0.9 and 5 pN. This dataset was very similar to that collected previously (Akiyoshi et al., 2010 & Figure S6), so the two datasets were combined for calculation of the wild-type statistics shown in Figures 5 & 6. A summary of all the data from force-clamp experiments is provided in Table S3.

Two-State Model

For the two-state kinetic scheme shown in Figure 5B, with the kinetochore initially bound to an assembling tip, the mean attachment lifetime, $\langle t \rangle$, is given by,

$$\langle t \rangle = \frac{k_1 + k_2 + k_4}{k_1 k_4 + k_2 k_3 + k_3 k_4},$$

as described previously (Akiyoshi et al., 2010). The rates, k_1, k_2, k_3, and k_4, represent the rates of catastrophe, rescue, detachment from assembling, and detachment from disassembling microtubules, respectively (the same rates displayed in Figure 5B). The predicted lifetime curves in Figure 6B were computed by substituting the best-fit exponential functions (Tables S2 and S3) into the equation above.

Table S1. Strains used in this study, related to all Figures.
All strains are derivatives of SBY3 (W303)

Strain	Relevant Genotype
SBY3 (W303)	*MAT*a *ura3-1 leu2-3,112 his3-11 trp1-1 can1-100 ade2-1 bar1-1*
SBY468	*MAT*a *lys2 trp1-1:: 256xlacO:TRP1 his3-11:pCUP1-GFP12-LacI12:HIS mad2Δ::URA3*
SBY2861	*MAT*a *STU2-13Myc:HIS3*
SBY8253	*MAT*a *DSN1-6His-3Flag:URA3*
SBY8944	*MAT*a *DSN1-6His-3Flag:URA3 DAD1::dad1-1:kanMX trp1-1::256xlacO:TRP1*
SBY10343	*MAT*a *DSN1-6His-3Flag:URA3 STU2-13Myc:HIS3*
SBY10345	*MAT*a *DSN1-6His-3Flag:URA3 STU2-13Myc:HIS3 DAD1::dad1-1:kanMX trp1-1::256xlacO:TRP1*
SBY10434	*MAT*a *DSN1-6His-3Flag:URA3 STU2-13Myc:HIS3 ndc80-1*
SBY10438	*MAT*a *DSN1-6His-3Flag:URA3 STU2-13Myc:HIS3 spc105-15*
SBY11709	*MAT*a *STU2-3V5:HisMX*
SBY11855	*MAT*a *DSN1-6His-3Flag:URA3 STU2-13Myc:HIS3 NDC80-3V5-IAA17:KanMX his3::pADH1-TIR1-9Myc:HIS3*
SBY11856	*MAT*a *DSN1-6His-3Flag:URA3 STU2-3V5-IAA7:KanMX DAM1-9Myc:TRP1 his3::pADH1-TIR1-9Myc:HIS3*
SBY11858	*MAT*a *DSN1-6His-3Flag:URA3 STU2-3V5-IAA7:KanMX DAM1-9Myc:TRP1*
SBY11860	*MAT*a *DSN1-6His-3Flag:URA3 STU2-3V5-IAA7:KanMX his3::pADH1-TIR1-9Myc:HIS3*
SBY12275	*MAT*a *STU2-3Flag:KanMX*
SBY13095	*MAT*a *STU2-6His-3Flag:URA3*
SBY13557	*MAT*a *STU2-3HA-IAA7:KanMX his3::pADH1-TIR1-9Myc:HIS3 leu2::pSTU2-STU2-3V5:LEU2*
SBY13772	*MAT*a *STU2-3HA-IAA7:KanMX DSN1-6His-3Flag:URA3 his3::pGPD1-TIR1:HIS3*

SBY13901	*MAT*a *STU2-3HA-IAA7:KanMX DSN1-6His-3Flag:URA3 his3::pGPD1-TIR1:HIS3 leu2::pSTU2-STU2-3V5:LEU2*
SBY14022	*MAT*a *SPC24-6His-3Flag:URA3 SPC105-3HA-IAA7:KanMX trp1::pGPD1-TIR1:TRP1*
SBY14584	*MAT*a *STU2-3HA-IAA7:KanMX DSN1-6His-3Flag:URA3 his3::pGPD1-TIR1:HIS3 NDC80-3V5-IAA7:KanMX*
SBY15985	*MAT*a *CDC20-IAA17:KanMX MTW1-3GFP:HIS3 ura3::TUB1-CFP:URA3 leu2::pGPD1-TIR1:LEU2*
SBY15986	*MAT*a *CDC20-IAA17:KanMX STU2-3HA-IAA7:KanMX MTW1-3GFP:HIS3 ura3::TUB1-CFP:URA3 leu2::pGPD1-TIR1:LEU2*
SBY16236	*MAT*a *lys2 trp1-1:: 256xlacO:TRP1 his3-11:pCUP1-GFP12-LacI12:HIS mad2Δ::URA3 STU2-3V5-IAA7:KanMX leu2::pGPD1-TIR1:LEU2*
SBY16239	*MAT*a *lys2 trp1-1:: 256xlacO:TRP1 his3-11:pCUP1-GFP12-LacI12:HIS STU2-3V5-IAA7:KanMX leu2::pGPD1-TIR1:LEU2*

Table S2. Parameters of the best-fit exponential functions, related to Figures 5, 6 & S6.
Parameters for exponential curve fits shown in Figure 5C-F, 6B & S6. The force dependence of all four rates, k_1, k_2, k_3, and k_4, was fit with the equation,

$$k_n(F) = k_n^o \ exp\{F/F_n\}$$

where F represents the applied force. The constants k_n^o and F_n represent the unloaded rate and the force required for an e-fold change, respectively.

wild-type	Transition	Unloaded rate k_n^o (hr^{-1})	Sensitivity F_n (pN)
	catastrophe (k_1)	6.1 ± 1.2	-2.9 ± 0.5
	rescue (k_2)	78 ± 19	5.4 ± 2.1
	detachment during assembly (k_3)	0.31 ± 0.1	3.7 ± 0.6
	detachment during disassembly (k_4)	205 ± 61	-2.1 ± 0.6

Stu2-AID	Transition	Unloaded rate k_n^o (hr^{-1})	Sensitivity F_n (pN)
	catastrophe (k_1)	6.1 ± 1.2	-2.9 ± 0.5
	rescue (k_2)	78 ± 19	5.4 ± 2.1
	detachment during assembly (k_3)	0.4 ± 0.2	1.1 ± 0.2
	detachment during disassembly (k_4)	3.7 ± 1.7	0.8 ± 0.2

Supplemental References

Burnette, W.N. (1981). "Western blotting": electrophoretic transfer of proteins from sodium dodecyl sulfate--polyacrylamide gels to unmodified nitrocellulose and radiographic detection with antibody and radioiodinated protein A. Anal. Biochem. *112*, 195–203.

Cheeseman, I.M., Anderson, S., Jwa, M., Green, E.M., Kang, J. seog, Yates, J.R., 3rd, Chan, C.S.M., Drubin, D.G., and Barnes, G. (2002). Phospho-regulation of kinetochore-microtubule attachments by the Aurora kinase Ipl1p. Cell *111*, 163–172.

Longtine, M.S., McKenzie, A., Demarini, D.J., Shah, N.G., Wach, A., Brachat, A., Philippsen, P., and Pringle, J.R. (1998). Additional modules for versatile and economical PCR-based gene deletion and modification in *Saccharomyces cerevisiae*. Yeast Chichester Engl. *14*, 953–961.

Pinsky, B.A., Kung, C., Shokat, K.M., and Biggins, S. (2006). The Ipl1-Aurora protein kinase activates the spindle checkpoint by creating unattached kinetochores. Nat. Cell Biol. *8*, 78–83.

Sarangapani, K.K., Akiyoshi, B., Duggan, N.M., Biggins, S., and Asbury, C.L. (2013). Phosphoregulation promotes release of kinetochores from dynamic microtubules via multiple mechanisms. Proc. Natl. Acad. Sci. U. S. A. *110*, 7282–7287.

Sarangapani, K.K., Duro, E., Deng, Y., Alves, F. de L., Ye, Q., Opoku, K.N., Ceto, S., Rappsilber, J., Corbett, K.D., Biggins, S., et al. (2014). Sister kinetochores are mechanically fused during meiosis I in yeast. Science *346*, 248–251.

Towbin, H., Staehelin, T., and Gordon, J. (1992). Electrophoretic transfer of proteins from polyacrylamide gels to nitrocellulose sheets: procedure and some applications. 1979. Biotechnol. Read. Mass *24*, 145–149.